Exploring uranium isotopes in shark teeth as a paleo-redox proxy

Haoyu Li [a,*], Michael A. Kipp [a], Sora L. Kim [b], Emma R. Kast [c], Jaelyn J. Eberle [d], François L.H. Tissot [a]

[a] *The Isotoparium, Division of Geological and Planetary Sciences, California Institute of Technology, Pasadena, CA, USA*
[b] *Department of Life and Environmental Sciences, University of California Merced, Merced, CA, USA*
[c] *Department of Earth Sciences, University of Cambridge, Cambridge, UK*
[d] *Department of Geological Sciences and Museum of Natural History, University of Colorado, Boulder, CO, USA*

ABSTRACT

The uranium isotope composition ($\delta^{238}U$) of seawater is a powerful proxy for the extent of marine anoxia. For paleoredox reconstructions, carbonates are the most popular U isotope archive, but they have recently come under increased scrutiny as their $\delta^{238}U$ values are subject to diagenetic alteration after deposition. Therefore, there is a need to investigate other archives that may record and preserve the original seawater $\delta^{238}U$ signal. In this study, we explore whether shark teeth provide such an archive. Shark teeth enameloid consisting of crystalline fluorapatite is more resistant to post-depositional alteration and less sensitive to isotopic exchange than marine carbonates due to the lower solubility of the crystalline fluorapatite. Since U is readily incorporated into phosphate, shark teeth could incorporate and preserve the original $\delta^{238}U$ signature of seawater.

To assess whether U isotopes in shark teeth can record seawater signatures, we measured the U isotopes (both $\delta^{238}U$ and $\delta^{234}U_{sec}$) in 39 fossil shark teeth from various locations, including Banks Island (Arctic), the Gulf of Mexico (GOM), and Pisco Basin (Peru), and ranging in age from modern to Cretaceous. Our results show that U concentrations are negligible in modern shark teeth (<1 ppb) but elevated in fossil samples (up to several hundred ppm), indicating that U is incorporated into shark teeth postmortem during burial. The $\delta^{238}U$ values range from -0.72 to $+0.57$ ‰, and the $\delta^{234}U$ values from -162.1 to $+969.7$ ‰. The data indicate that (i) diagenetic overprinting of seawater U isotope ratios is common among shark teeth, and (ii) $\delta^{238}U$ data are influenced by local depositional environments. Nonetheless, the U isotope variations observed in shark teeth are comparable to those seen in marine carbonates, indicating that the samples with less diagenetic alterations might offer useful insight into the past extent of ocean anoxia.

1. Introduction

Biogenic phosphates are regarded as a valuable geochemical archive offering insight into a wide range of paleoceanographic conditions and processes, such as temperature, salinity, and water mass circulation (*e.g.,* Longinelli, 1966; Kolodny et al., 1983; Reynard et al., 1999; Kohn and Cerling, 2002; Martin and Scher, 2004; Ounis et al., 2008; Fischer et al., 2013; Huck et al., 2016). Shark teeth are among the most extensively studied marine biogenic phosphates due to their ability to record and retain geochemical signatures on geological timescales. Sharks have existed on Earth for over 400 Myr, and the oldest shark fossils date from the early Devonian (Miller et al., 2003), with continuous records to the present and wide spatial distribution (Ginter et al., 2010). Because sharks are Chondrichthyes (cartilaginous fish), shark skeletons largely decompose before fossilization, making shark teeth their most abundant fossil record. With lifelong continuous tooth replacement, sharks can produce thousands of teeth throughout their lifetime (Botella et al., 2009). Once shark teeth are lost from their bodies, they interact with ambient water and incorporate elements from the surrounding environment. Due to the rapid mineralization on daily to weekly timescales, shark teeth can even capture local geochemical snapshots of the sites from which they originate (Kolodny et al., 1991; Picard et al., 1998; Vennemann et al., 2001; Lécuyer et al., 2003; Pucéat et al., 2003; Martin and Scher, 2004; Dera et al., 2009; Kocsis et al., 2009; Fischer et al., 2012; Kim et al., 2014, 2020).

Shark teeth enameloid tissues are primarily composed of fluorapatite (Enax et al., 2012), a calcium phosphate with extremely low solubility (Moreno et al., 1974), making them more resistant to post-depositional

---

* Corresponding author.
  E-mail address: haoyu.li@caltech.edu (H. Li).

alterations than other popular paleoceanographic archives such as carbonates (Kolodny et al., 1983; Shemesh et al., 1983; Kolodny and Raab, 1988; Iacumin et al., 1996; Zazzo et al., 2004a; Lécuyer et al., 2013). Shark teeth are composed of two types of tissue: enameloid (enamel-like outer layer) and dentine (mineralized but organic-rich inner core) (Fig. 1). Enameloid is considered to be a more robust archive for geochemical proxies because of its higher apatite content, fluorapatite mineralogy, lower water and organic matter content, and more compact structure with larger phosphate crystallites (Kohn et al., 1999; Sharp et al., 2000; Kohn and Cerling, 2002; Zazzo et al., 2004b; Enax et al., 2012). These characteristics have led to the successful application of geochemical tracers in shark teeth to understand paleo-environmental conditions and the behavior of sharks.

Several isotopic tracers have been well-studied in the enameloid of shark teeth. Oxygen isotopes are the most widely-studied system, being frequently used to track paleotemperature and paleosalinity (Kolodny and Raab, 1988; Kolodny et al., 1991; Lécuyer et al., 1993, 2003; Picard et al., 1998; Vennemann and Hegner, 1998; Sharp et al., 2000; Vennemann et al., 2001; Pucéat et al., 2003; Ounis et al., 2008; Dera et al., 2009; Kocsis et al., 2009, 2014; Fischer et al., 2012, 2013; Kim et al., 2014, 2020; Hättig et al., 2019). Strontium isotopes are used for chemostratigraphic dating of shark teeth, as well as for understanding freshwater/brackish habitat preference and migration history (Schmitz et al., 1991, 1997; Vennemann and Hegner, 1998; Barrat et al., 2000; Martin and Haley, 2000; Vennemann et al., 2001; Kocsis et al., 2007, 2009, 2013; Becker et al., 2008; Fischer et al., 2012, 2013; Bosio et al., 2020; Tütken et al., 2020). Additionally, the neodymium isotope composition of shark teeth is extensively used as a paleocirculation tracer (Shaw and Wasserburg, 1985; Vennemann and Hegner, 1998; Martin and Haley, 2000; Vennemann et al., 2001; Kocsis et al., 2007, 2009; Huck et al., 2016; Kim et al., 2020). These broad applications of shark teeth motivated our exploration of this archive to track the extent of marine anoxia in deep time.

The redox history of surface environments is of interest in paleo-environmental studies because of its cause-effect relationships with the evolution of life on Earth. In recent years, uranium (U) isotopes ($^{238}U/^{235}U$, expressed in delta notation as $\delta^{238}U$) have become one of the most powerful quantitative tools for reconstructing marine redox variations (e.g., Zhang et al., 2020, and references therein). U has two oxidation states in the terrestrial surface environment: insoluble U(IV) and soluble U(VI) (Langmuir, 1978). The U input to the ocean is dominated by riverine U(VI) input from weathering, which is isotopically indistinguishable from continental crust ($\delta^{238}U = -0.29 \pm 0.03$ ‰, Tissot and Dauphas, 2015; Andersen et al., 2016). In anoxic/euxinic settings, U(VI) is efficiently removed from the water column via

reductive precipitation as U(IV) in uraninite by abiotic and/or biotic reductions (Langmuir, 1978). During the U(VI) removal processes, ^{238}U (relative to ^{235}U) is preferentially incorporated into the sediments (Andersen et al., 2017). As a result, in periods of expanded marine anoxia the rate of U burial increases, causing seawater to shift toward lower U concentration and $\delta^{238}U$ value.

Importantly, U isotopes are considered a proxy for the global extent of marine anoxia. In the well-oxygenated modern ocean, the long residence time of U ($\tau \sim 400$ kyr, Ku et al., 1977; Dunk et al., 2002), much longer than global ocean mixing time (~1 kyr, Broecker and Peng, 1982) results in both homogeneous salinity-normalized concentration (~3.2 ng/g for a salinity of 35 g/L, Chen et al., 1986; Owens et al., 2011) and isotopic composition ($\delta^{238}U = -0.379 \pm 0.023$ ‰, Tissot and Dauphas, 2015; Kipp et al., 2022). Thus, any geological archive that faithfully records the ambient seawater $\delta^{238}U$ value can be used to infer the global extent of marine anoxia in deep time.

Carbonate sediments are the most popular archive used in such reconstructions to-date as they are abundant in the geologic record, contain ample U, and tend to record the seawater $\delta^{238}U$ signature upon precipitation (Stirling et al., 2007; Weyer et al., 2008; Romaniello et al., 2013; Tissot and Dauphas, 2015; Chen et al., 2016, 2018a; Tissot et al., 2018; Kipp et al., 2022). However, carbonates are subject to syndepositional and post-depositional diagenetic alterations, which can overprint the original $\delta^{238}U$ signatures, posing a significant challenge for this archive (Romaniello et al., 2013; Chen et al., 2018a; Tissot et al., 2018; Livermore et al., 2020). This diagenetic overprinting complicates quantitative paleoredox reconstructions (Kipp and Tissot, 2022), undermining the utility of carbonates as a U isotope archive. While such diagenetic modifications also commonly exist in bioapatite (Toyoda and Tokonami, 1990; Tütken et al., 2011), shark teeth enameloid is nevertheless thought to be more resistant to post-depositional alteration than carbonate (Zazzo et al., 2004b).

The objective of this study is to explore shark teeth as a novel archive of seawater $\delta^{238}U$, leveraging the diagenetic stability of apatite over carbonate. We first report U isotope compositions of a variety of modern and fossil shark teeth (from both enameloid and dentine tissues) and the sediments in which they are embedded. Bulk U and Th concentrations, in-situ U concentration transition profiles, and phosphate $\delta^{18}O$ values are then used to understand the diagenetic history of these shark teeth and assess the corresponding implications for their promise as a seawater U isotope archive.

2. Methods

2.1. Geological settings and materials

In this work, 39 fossil shark teeth, 6 modern teeth, and 7 sediment samples were analyzed (Table 1). Fossil shark teeth were mainly selected from three locations: Banks Island, the Gulf of Mexico, and the Pisco Basin (called the Arctic, GOM, and Peru hereafter respectively, Fig. 2). The Arctic shark teeth housed at the Canadian Museum of Nature belong to *Striatolamia macrota*, and were recovered as float on unconsolidated sands in the Cyclic Member of the Eureka Sound Formation (Aulavik National Park, northern Banks Island, Northwest Territories, Canada, ca. 74° N, Padilla et al., 2014). Shark teeth from this locality were deposited in a shallow coastal marine delta front environment (Miall, 1979), with a stratigraphic age of early Eocene (ca. 51–53 Ma) based on palynology (Sweet, 2012). The GOM shark teeth are *Carcharias hopei*, which were collected from the Eocene Jackson Group in Polk County, Texas, USA, and the late Eocene Clinchfield Formation in Gordon, Wilkinson County, Georgia, USA (specimens are from the Texas Vertebrate Paleontology Collection at the University of Texas, Austin). Peruvian shark teeth are from *Cosmopolitodus hastalis*, which were recovered as float on unconsolidated sandstone from the Pisco Formation in the Province of Caravelí, Peru, whose depositional environment is shallow marine spanning protected coastal to offshore shelf habitats (Ehret et al., 2012; Ochoa
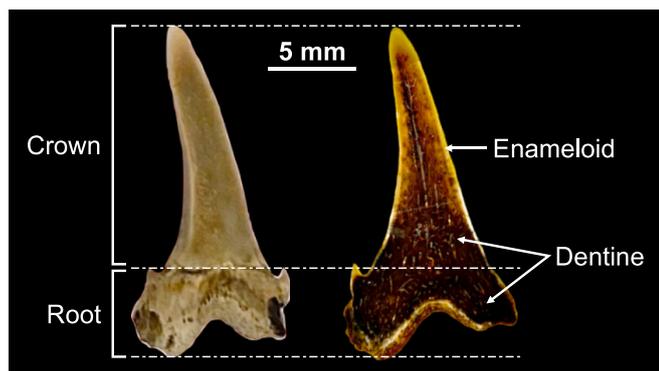

Fig. 1. Histology of shark tooth. Photo (left) and transmitted light microscope image of polished cross section (right) of a *Striatolamia macrota* shark tooth from the Banks Island in the Arctic. Enameloid forms a thin translucent layer covering the crown, while dentine forms the crown base and the root of the tooth. The junction between enameloid and dentine is clear, and the dentine is more porous than enameloid.

Table 1
Summary of locality, formation, age, U isotope compositions, U and Th concentrations, U/Th ratios, and O isotope composition of shark teeth and sediments measured in this study.

Sample	Locality	Formation	Age	δ238U (‰)	95 % CI	δ234Usec (‰)	95 % CI	U (ng)	n	[U] (ppm)	[Th] (ppm)	U/Th (ppm/ppm)	δ18OPO4 (‰ VSMOW)	±SD
Enameloid														
Banks Island (Arctic)														
2004-31-01	Banks Island, BC, Canada	Eureka	Eocene	−0.41	0.07	753.7	0.4	108	6	3.96	36.78	0.108	16.1	0.4
2004-31-02	Banks Island, BC, Canada	Eureka	Eocene	−0.38	0.05	444.2	0.5	162	9	10.25	53.12	0.193	11.6	0.6
2004-31-03	Banks Island, BC, Canada	Eureka	Eocene	−0.68	0.05	197.1	0.5	162	9	8.76	32.07	0.273	10.4	0.2
2004-31-04	Banks Island, BC, Canada	Eureka	Eocene	−0.56	0.05	226.4	0.5	162	9	17.50	63.63	0.275	10.4	0.2
2004-31-05	Banks Island, BC, Canada	Eureka	Eocene	−0.39	0.06	668.0	0.6	108	6	4.44	38.89	0.114	11.0	0.9
2004-31-06	Banks Island, BC, Canada	Eureka	Eocene	−0.43	0.05	143.1	0.5	162	9	27.64	101.27	0.273	10.9	0.3
SLK2004-13-4	Banks Island, BC, Canada	Eureka	Eocene	−0.32	0.07	814.8	0.4	108	6	5.54	54.62	0.101	9.1	0.1
SLK2004-13-3	Banks Island, BC, Canada	Eureka	Eocene	−0.44	0.07	310.9	0.4	108	6	5.46	36.08	0.151	18.5	0.1
SLK2004-13-1	Banks Island, BC, Canada	Eureka	Eocene	−0.57	0.08	969.7	0.4	90	5	2.61	25.25	0.103		
BKS04-19	Banks Island, BC, Canada	Eureka	Eocene	−0.66	0.11	925.3	1.0	36	2	2.16	15.49	0.139		
BKS2004-31	Banks Island, BC, Canada	Eureka	Eocene	−0.42	0.06	450.3	0.5	126	7	3.32	28.77	0.115		
Gulf of Mexico (GOM)														
TxVP 43390-2.102	Wilkinson Co, GA, USA	Clinchfield	late Eocene	0.03	0.07	−30.6	0.4	108	6	2.09	3.09	0.678	21.5	0.7
TxVP 43390-2.201	Wilkinson Co, GA, USA	Clinchfield	late Eocene	0.21	0.11	−40.0	0.5	54	3	320.30	50.09	6.394	21.5	0.5
TxVP 43390-2.85	Wilkinson Co, GA, USA	Clinchfield	late Eocene	0.17	0.07	−126.3	0.4	108	6	17.53	4.78	3.669	22.1	0.2
TxVP 43390-2.252	Wilkinson Co, GA, USA	Clinchfield	late Eocene	−0.04	0.06	−14.2	0.3	162	9	3.16	1.95	1.617	21.8	0.1
TxVP 43390-2.218	Wilkinson Co, GA, USA	Clinchfield	late Eocene	0.04	0.07	−133.8	0.4	108	6	6.87	3.31	2.077	21.8	0.2
TxVP 43390-2.235	Wilkinson Co, GA, USA	Clinchfield	late Eocene	0.27	0.07	−162.1	0.4	108	6	14.17	5.29	2.677	22.5	0.1
TxVP 40278-1-01	Polk Co., TX, USA	Jackson	Eocene	−0.44	0.06	243.5	0.3	198	11	11.60	15.51	0.748	19.5	0.3
TxVP 40278-1-02	Polk Co., TX, USA	Jackson	Eocene	0.50	0.05	−11.5	0.5	162	9	31.07	1.62	19.12	19.8	0.2
TxVP 40278-1-BB	Polk Co., TX, USA	Jackson	Eocene	−0.37	0.05	292.5	0.5	144	8	28.39	14.49	1.959	19.2	0.4
TxVP 45995-1-01	GA, USA	Clinchfield	late Eocene	0.27	0.11	−48.1	0.5	54	3	32.15	1.30	24.75	24.0	0.8
TxVP 45995-1-02	GA, USA	Clinchfield	late Eocene	−0.53	0.05	448.6	0.5	162	9	20.66	9.32	2.216	23.3	0.2
TxVP 45995-1-03	GA, USA	Clinchfield	late Eocene	0.57	0.05	−17.7	0.5	162	9	45.09	2.00	22.51	23.4	0.1
Pisco Basin (Peru)														
P1007-01	Bella Unión, Caravelí, Peru	Pisco	Late Miocene	−0.26	0.06	15.5	0.3	144	8	3.16	1.26	2.517	23.2	0.1
P1007-02	Bella Unión, Caravelí, Peru	Pisco	Late Miocene	−0.03	0.06	8.5	0.6	108	6	4.08	3.92	1.039	22.5	0.1
P1007-03	Bella Unión, Caravelí, Peru	Pisco	Late Miocene	−0.05	0.06	−4.5	0.6	108	6	4.72	8.21	0.574	22.2	0.1
P1007-04	Bella Unión, Caravelí, Peru	Pisco	Late Miocene	−0.72	0.09	151.4	0.8	54	3	2.56	0.43	6.002	20.2	0.5
LMS001-05	Bella Unión, Caravelí, Peru	Pisco	Late Miocene	−0.05	0.07	86.5	0.4	108	6	6.23	11.95	0.521		
LMS001-08	Bella Unión, Caravelí, Peru	Pisco	Late Miocene	−0.28	0.11	−16.1	0.5	54	3	67.32	4.08	16.50	21.2	0.1
JAH001-02	Bella Unión, Caravelí, Peru	Pisco	Late Miocene	−0.16	0.07	63.2	0.4	108	6	23.21	0.18	129.5	21.6	0.3
JAH001-03	Bella Unión, Caravelí, Peru	Pisco	Late Miocene	−0.23	0.07	517.7	0.4	108	6	3.82	0.02	160.5	22.3	0.5
SS001-04	Bella Unión, Caravelí, Peru	Pisco	Late Miocene	−0.41	0.13	44.9	0.7	36	2	1.22	1.39	0.882	21.0	0.4
SCM001-05	Bella Unión, Caravelí, Peru	Pisco	Late Miocene	−0.08	0.05	5.1	0.3	216	12	8.34	1.62	5.154	22.2	0.2
SCM001-06	Bella Unión, Caravelí, Peru	Pisco	Late Miocene	−0.04	0.07	−31.7	0.4	108	6	5.16	7.54	0.685	22.1	0.2
CMTR001-04	Bella Unión, Caravelí, Peru	Pisco	Late Miocene	−0.29	0.11	−6.8	0.5	54	3	38.39	1.77	21.69	21.8	0.2
Other fossil teeth														
279,414	Lee Creek Mine, NC, USA	Yorktown	Pliocene	−0.12	0.04	−84.6	0.2	82	7	16.60	0.02	689.1		
444242-2	Howell Park, NJ, USA	Kirkwood	Miocene	−0.52	0.04	26.6	0.8	23	2	1.23	0.08	15.13		
F*t-2e	Ramenessin Brook, NJ, USA		Cretaceous*	−0.38	0.03	−1.1	0.2	105	9	59.70	2.33	25.67		
EK digest1	North Carolina, USA*		Pliocene*	−0.32	0.02	0.8	0.3	152	13	115.40	0.15	772.9		
EK digest2	North Carolina, USA*		Pliocene*	−0.30	0.02	0.9	0.3	140	12	105.50	0.14	780.7		
EK digest3	North Carolina, USA*		Pliocene*	−0.30	0.02	0.8	0.3	129	11	100.90	0.13	774.3	22.4	0.4
EK digest4	North Carolina, USA*		Pliocene*	−0.29	0.03	1.6	0.2	105	9	97.60	1.82	53.6	22.7	0.4
EK average				−0.31	0.01	1.2	0.1							
Dentine														
P1007-01_D	Bella Unión, Caravelí, Peru	Pisco	Late Miocene	−0.41	0.05	51.4	0.5	162	9	65.38	0.04	1839.1		
LMS001-08_D	Bella Unión, Caravelí, Peru	Pisco	Late Miocene	−0.29	0.05	−30.3	0.5	144	8	145.45	3.98	36.50		
SS001-04_D	Bella Unión, Caravelí, Peru	Pisco	Late Miocene	−0.37	0.05	180.3	0.5	144	8	106.10	0.62	171.0		
SCM001-06_Dc	Bella Unión, Caravelí, Peru	Pisco	Late Miocene	−0.20	0.05	−53.6	0.5	162	9	48.30	17.97	2.688		

(continued on next page)

Table 1 (*continued*)

Sample	Locality	Formation	Age	$\delta^{238}U$ (‰)	95 % CI	$\delta^{234}U_{sec}$ (‰)	95 % CI	U (ng)	n	[U] (ppm)	[Th] (ppm)	U/Th (ppm/ppm)	$\delta^{18}O_{PO4}$ (‰ VSMOW)	±SD
SCM001-06_Dr	Bella Unión, Caravelí, Peru	Pisco	Late Miocene	−0.25	0.05	−71.5	0.5	144	8	149.85	42.81	3.500		
TMM40278-1-BB_D	Polk Co., TX, USA	Jackson	Eocene	−0.36	0.05	287.5	0.5	162	9	64.55	8.81	7.323		
Sediments														
BKS04-19_sed	Banks Island, BC, Canada	Eureka	Eocene	−0.56	0.04	101.1	0.3	288	16	1.71	1.67	1.023		
BKS2004-31_sed	Banks Island, BC, Canada	Eureka	Eocene	−0.27	0.04	−2.9	0.4	234	13	0.98	2.46	0.399		
JAH010_sed	Bella Unión, Caravelí, Peru	Pisco	Late Miocene	−0.24	0.04	128.1	0.3	306	17	2.50	5.67	0.441		
JBL002_sed	Bella Unión, Caravelí, Peru	Pisco	Late Miocene	1.38	0.04	457.8	0.3	306	17	13.51	4.56	2.965		
SS003_sed	Bella Unión, Caravelí, Peru	Pisco	Late Miocene	−0.45	0.04	142.2	0.3	306	17	3.36	1.47	2.296		
SCM002_sed	Bella Unión, Caravelí, Peru	Pisco	Late Miocene	−0.06	0.04	64.4	0.3	288	16	20.25	5.84	3.466		
P1002_sed	Bella Unión, Caravelí, Peru	Pisco	Late Miocene	−0.16	0.04	22.3	0.3	288	16	1.09	4.11	0.264		
Geostandard														
BCR-2 digest1				−0.21	0.05	−0.1	1.3	162	9					
BCR-2 digest2				−0.25	0.04	0.6	0.4	198	11					
BCR-2 digest3				−0.21	0.07	0.3	0.6	90	5					
BCR-2 digest4				−0.26	0.06	0.3	0.6	108	6					
BCR-2 digest5				−0.25	0.09	0.4	0.8	54	3					
BCR-2 average				−0.236	0.028	0.32	0.25							

The "*" indicates the locality or the age are indeterminate.
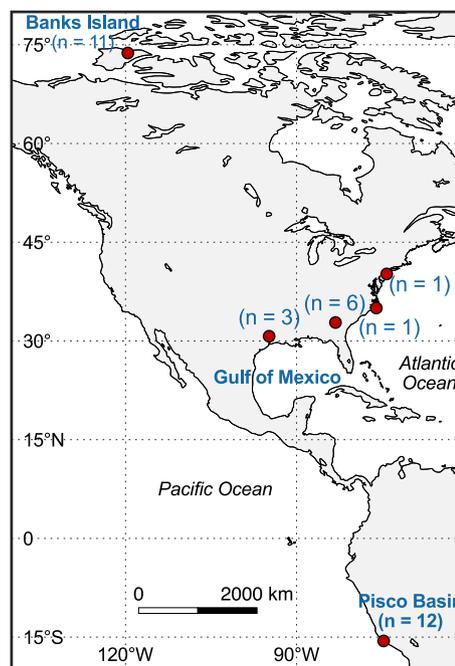
Fig. 2. Map showing the localities of the fossil shark teeth and sediments used in this study. The samples are primarily from 3 locations: Banks Island (Arctic), the Gulf of Mexico (GOM), and Pisco Basin (Peru), with a few others scattered on the east coast of the US.

et al., 2021) with a stratigraphic age of Late Miocene. Prior work (Wang et al., 2016; Gothmann et al., 2019) has suggested that there was little change in the seawater $\delta^{238}U$ value over the Cenozoic, meaning well-preserved primary signatures should resemble the modern value. For modern shark teeth, the sources include collections from Gordon Hubbel and Lisa Natanson, purchase from eBay.

The shark teeth investigated here show the same histology as described in previous literature, which consists of two tissues: enameloid and dentine (Fig. 1). The highly crystalline enameloid forms a thin compact outer layer covering the crown of the tooth, whereas the less crystalline and more porous dentine comprises the pulp cavity and the root structure of the shark tooth.

2.2. Sample preparation

For the fossil shark teeth from the Arctic, GOM, and Peru, enameloid was carefully abraded from each fossil shark tooth with a clean razor blade to avoid contamination from other tissues. Small chunks of dentine and sediments were also extracted and individually ground with pestle and agate mortar for isotopic analysis. All tools used in the extraction were cleaned with ethanol before and after sampling each tooth and sediments sample. For other fossil teeth from New Jersey and North Carolina, either enameloid chips were taken from the teeth with any dentine on the inside surface removed with a Dremel tool, or the enameloid powder was directly drilled from the surface of the teeth.

Wet chemistry and isotopic measurements were performed at the Isotoparium (Caltech). All digestions and dilutions used trace-metal-clean acids (purified via two rounds of sub-boiling distillation) and acid-cleaned PFA beakers. Enameloid (10–40 mg), dentine (5–70 mg), and sediments (160–200 mg) were weighed in clean 7 mL PFA beakers, and then dissolved by consecutive acid attack: 5 mL concentrated 3:1(v/v) $HF:HNO_3$ at 130 °C for 24 h followed by 5 mL concentrated aqua regia at 140 °C for 24 h. Between the two acid attacks, 100 μL concentrated $HClO_4$ were added to dried samples to dissolve residual fluorides, and then the $HClO_4$ was removed by heating at 165 °C for several hours. These steps were repeated to ensure complete dissolution. After

digestion, samples were dried and redissolved into concentrated HNO_3, then brought up in 5 mL of 3 M HNO_3. A 2–3 % aliquot was taken from the digest for concentration analysis on an iCAP RQ ICPMS (Thermo-Fisher). Based on [U] data, samples were spiked with IRMM-3636 to obtain U_{spike}/U_{sample} ratios of 3–5 % (Tissot et al., 2019). The spiked solutions were dried completely and taken back into 1 mL concentrated HNO_3. The samples were refluxed on a hotplate at 130 °C to ensure the sample and spike were well equilibrated and then diluted to 5 mL 3 M HNO_3 for column chemistry. To monitor long-term external reproducibility, several powder aliquots of geostandard BCR-2 were digested in parallel to the shark teeth and sediment samples.

Uranium purification was performed on pre-packed 2 mL U-TEVA cartridges (Eichrom) following established methods (Tissot and Dauphas, 2015; Tissot et al., 2016, 2017). In brief, the resin was cleaned with 40 mL 0.05 M HCl, and then conditioned with 10 mL 3 M HNO_3. Samples were loaded onto the resin in 5 mL 3 M HNO_3, and matrix elements were eluted in 12 mL 3 M HNO_3. The resin was then converted with 5 mL 10 M HCl, followed by Th removal in 8 mL 5 M HCl. U was finally eluted in 20 mL 0.05 M HCl and collected in cleaned 30 mL beakers. The U cut was evaporated to dryness, and 0.25 mL H_2O_2 and 0.20 mL concentrated HNO_3 were added to oxidize any organic matter released from the resin. After refluxing overnight at 120 °C, the mixture was completely dried and taken back into 3 M HNO_3. The column chemistry was repeated a second time to ensure precise and accurate measurements of $^{234}U/^{238}U$ (Tissot et al., 2018). Uranium procedural blank ~13 pg (<0.04 % of U in sample) and are therefore negligible. The final U cuts were evaporated to dryness before being redissolved in concentrated HNO_3. Samples were then evaporated to near dryness, and ultimately diluted to 3 vol% HNO_3 for isotopic measurements.

2.3. Mass spectrometry

All U isotope analyses were performed on a Neptune*Plus* (Thermo-Fisher) multiple collector inductively coupled plasma mass spectrometer (MC-ICPMS) at Caltech, following established methods (Tissot and Dauphas, 2015; Kipp et al., 2022). The Jet sample and X-skimmer cones were used in combination with an *Aridus3* or Apex Omega HF desolvating nebulizer. The measurements were conducted in low-resolution mode using a static cup configuration. Each analysis consisted of 50 cycles of 4.194 s integration time. The sample measurements were bracketed by the CRM-112a standard spiked with IRMM-3636 at a similar U_{spike}/U_{sample} ratio as the samples. Instrumental mass fractionation was corrected by standard-sample-bracketing and double spike deconvolution. Amplifier gain calibrations were performed daily. The ^{234}U signal was measured with a secondary electron multiplier (SEM) on the axial mass. The SEM-Faraday cup gain was calibrated manually with replicate analyses of the CRM-112a standard solution in both SEM and Faraday mode at the beginning and end of each analytical sequence (Kipp et al., 2022).

The $^{238}U/^{235}U$ ratios are reported in δ-notation relative to the standard CRM-112a (CRM-145 for the solution form, $^{238}U/^{235}U = 137.837$, Richter et al., 2010), which is defined as:

$$\delta^{238}U = \left(\frac{^{238}U/^{235}U_{smp}}{^{238}U/^{235}U_{CRM-112a}} - 1 \right) \times 1000 \tag{1}$$

The $^{234}U/^{238}U$ ratios are reported as $\delta^{234}U_{sec}$, relative to secular equilibrium as:

$$\delta^{234}U_{sec} = \left(\frac{^{234}U/^{238}U_{smp}}{^{234}U/^{238}U_{Sec.\ Eq}} - 1 \right) \times 1000 \tag{2}$$

where $^{234}U/^{238}U_{Sec.\ Eq}$ denotes the atomic ratio at secular equilibrium, which is the ratio of the decay constants of ^{238}U and ^{234}U, $\lambda_{238}/\lambda_{234} = (1.55125 \times 10^{-10})/(2.8220 \times 10^{-6}) = 5.4970 \times 10^{-5}$ (Cheng et al., 2013). Uncertainties are reported as 2SE (95 % CI) and calculated using

the daily external reproducibility of the CRM-112a standard (2SD) divided by the square root of the number of replicate measurements for a given sample (i.e., $2SE = 2SD_{External}/\sqrt{n}$). Depending on the available material, each sample was analyzed 3 to 17 times. Replicate measurements of the BCR-2 basalt geostandard gave an average $\delta^{238}U$ of -0.236 ± 0.026 ‰ and $\delta^{234}U_{sec}$ of $+0.32 \pm 0.25$ ‰ ($n_{digests} = 5$, $n_{analyses} = 34$), within the uncertainty of the recommend $\delta^{238}U$ value of -0.262 ± 0.004 ‰, calculated using all previously published high-precision data (data from the uranium isotope database, Li and Tissot, 2023).

2.4. LA-ICPMS

Elemental concentration profiles across shark teeth sections were measured *in-situ* by laser ablation inductively coupled plasma mass spectrometry (LA-ICPMS) at the Isotoparium. Selected shark teeth samples were mounted in 1 in. of epoxy and polished prior to analysis. Concentrations were measured using an iCAP RQ ICPMS coupled with a NWRfemto laser ablation system (Elemental Scientific). Laser sampling was conducted at $\lambda = 257$ nm, with 30 % energy output. The spot size and repetition rate were set to 40 μm and 20 Hz, respectively. The measurements were conducted in linear scan mode, with a scan speed of 10 μm/s. Data reduction followed the method in Longerich et al. (1996), and the uranium concentrations were calculated as:

$$[U]_{smp} = \frac{n(U)_{smp}}{\frac{n(U)_{NIST616}}{[U]_{NIST616}} \times \left(\frac{n(Ca)_{smp}}{n(Ca)_{NIST616}} \times \frac{[Ca]_{NIST616}}{[Ca]_{smp}} \right)} \tag{3}$$

where n is the background corrected count rate, with units of counts per second (cps). The international glass reference material NIST616 was used for external calibration, assuming a CaO content of 12 wt% (Kane, 1998) and U concentration of 0.0721 ppm. Calcium was used as the internal standard to correct the variations in mass ablation yield, assuming shark teeth with an average apatite CaO value of 53 wt% (Trotter and Eggins, 2006).

2.5. O isotopes

The enameloid powder was gently abraded from each tooth using a razor blade. The sampling tools were cleaned with ethanol before each sample collection. To analyze the phosphate oxygen isotope composition, we followed the rapid, small volume preparation methodology of Mine et al. (2017). Briefly, ~1 mg of enameloid powder was weighed and dissolved in 50 μL 2 M HNO_3 overnight. Then, 30 μL of 2.9 M HF and 50 μL of 2 M NaOH were added to precipitate CaF_2 and supernatant removed to a separate vial. The CaF_2 pellet was rinsed with 50 μL 0.1 M NaF and this second aliquot of supernatant was added to the separate vial. Before precipitating the Ag_3PO_4, the pH was adjusted to 4.5 with 2 M HNO_3 (~30 μL), then 180 μL of Ag ammine solution (1.09 M NH_4OH and 0.37 M $AgNO_3$; pH of 5.5–6.5 after addition of Ag-ammine solution) was added; crystals precipitated and settled for 5–7 min. Finally, we centrifuged samples to pellet the silver phosphate crystals and rinsed the samples five times with deionized water. Samples were dried overnight at 60 °C and weighed in triplicate to 300 ± 100 μg into silver capsules for isotopic analysis. The measurements were performed at the Stable Isotope Ecosystem Laboratory of University of California, Merced (SIELO) using a Temperature Conversion Elemental Analyzer (TC/EA) coupled with a Conflo IV to a Thermo Scientific Delta V continuous flow isotope ratio mass spectrometer (CF-IRMS). The O isotope compositions ($\delta^{18}O_{PO4}$) are reported relative to the standard V-SMOW using silver phosphate standards USGS 80 ($n = 15$; $1\sigma = 0.4$) and USGS 81 ($n = 14$; $1\sigma = 0.5$) for normalization, drift, and linearity corrections. A preparation check standard (IAEA 601) resulted in $\delta^{18}O$ values = $+23.0 \pm 0.2$ ‰ and analytical corrections were checked with an in house Ag_3PO_4 reference material (Alfa Aesar; n = 2, $\Delta = 0.2$). Each sample was measured three times, with uncertainty reported as the standard

deviation of the triplicate analyses.

3. Results

3.1. U concentration

Considering first the U concentrations of enameloid tissues only, the data show that modern and fossil shark teeth define two populations (Fig. 3). Modern teeth are characterized by low U concentrations (in the ppb range), whereas the 43 fossil shark teeth display values at or above the ppm level, at least four orders of magnitude higher than modern teeth. The U concentrations in enameloid tissues of fossil teeth are highly variable (1.2–320 ppm), and no clear trend in U concentrations is observed with sample age or locality.

In fossil teeth, U concentrations of enameloid and dentine tissues were determined by both bulk solution (n = 5; Fig. 4a) and *in-situ* methods (n = 2; Fig. 4b). Bulk measurements conducted on 5 shark teeth show that [U] of enameloid range from 1.2 to 67 ppm, and dentine from 48 to 150 ppm. In the same tooth, U concentrations are always lower in the enameloid compared to dentine, in agreement with previous literature (Kohn et al., 1999; Tütken et al., 2020). The U concentration variations also exist between different segments of the same tissue, as shown by the lower concentration seen in the crown dentine than in the root dentine.

In-situ measurements corroborate the results of the bulk analyses. The U concentration profile based on LA-ICPMS through the cross-section of fossil shark teeth crown varies and delineates differences between the enameloid and dentine (Fig. 4b, S2b). Dentine is enriched in U compared to the enameloid, and compositional variations within the same tissue are also observed. The [U] profile in the dentine is noisy, with concentrations ranging from ~40 to 120 ppm, while values in enameloid decrease from the inner side (contact with dentine) to the outer side.

3.2. U isotopes

3.2.1. Shark teeth enameloid and sediments

The U isotope compositions of fossil shark teeth tissues and sediments are shown in Table 1 and Fig. 5. Owing to the extremely low U content of modern teeth, isotopic analyses were not possible on these samples. To test the if U isotope heterogeneity exists in enameloid tissues, four aliquots were taken from a large *Otodus megalodon* tooth (EK) and digested separately for isotopic analyses. The $\delta^{238}U$ values of the replicated digests are indistinguishable within the uncertainty (Table 1 and Fig. S3). Small variabilities (<1 ‰) are observed in $\delta^{234}U_{sec}$ values, but this intra-tooth variability is much smaller than those among different shark teeth.

The $\delta^{238}U$ values of enameloid from fossil shark teeth vary from −0.72 to +0.57 ‰, a range comparable to that observed in Cenozoic
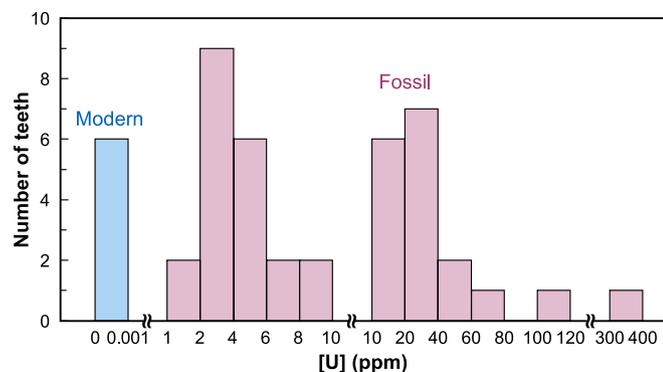

Fig. 3. Histogram of U concentrations in enameloid tissues of modern and fossil shark teeth.

carbonates (Romaniello et al., 2013; Tissot and Dauphas, 2015; Chen et al., 2018a, b, 2021; Tissot et al., 2018; Gothmann et al., 2019; Bura-Nakić et al., 2020; Livermore et al., 2020). The $\delta^{234}U_{sec}$ values cover a very wide range, from −162.1 to +969.7 ‰, showing departures both below and (far) above secular equilibrium, which testify to recent open-system behavior and exchange of ^{234}U.

In the Arctic, $\delta^{238}U$ values range from −0.68 to −0.32 ‰, showing limited variation near the modern seawater value. The $\delta^{234}U_{sec}$ values of these samples range from +143.1 to +969.7 ‰, displaying the largest range among the three studied localities. For two of these teeth (BKS04-19 and BKS2004-31), the embedding sediments were analyzed. The shark teeth enameloid and embedding sediments show similar $\delta^{238}U$ values within analytical uncertainties ($\Delta_{enamel-sed} < 0.15$ ‰). In contrast, the sediments have $\delta^{234}U_{sec}$ values of −2.9 to +101.1 ‰, much lower than that of the shark teeth they surround.

Shark teeth from Peru have $\delta^{238}U$ and $\delta^{234}U_{sec}$ values ranging from −0.72 to −0.03 ‰ and −31.7 to +517.4 ‰, respectively. Most sediments from Peru cover similar ranges of both $\delta^{238}U$ and $\delta^{234}U_{sec}$, with one exception, sediment JBL002-sed, which is characterized by the highest $\delta^{238}U$ value measured in this study of +1.38 ‰.

Samples from GOM have a larger range of $\delta^{238}U$ values, from −0.53 to +0.57 ‰ and have $\delta^{234}U_{sec}$ between −162.1 and +448.6 ‰. For this locality, no sediments were available for comparative analysis. The remaining fossil shark teeth, which originated from North Carolina and New Jersey, USA (orange symbols in Fig. 5a), show more limited variations in $\delta^{238}U$ and $\delta^{234}U_{sec}$.

3.2.2. Enameloid and dentine

Similar to U concentration, U isotopes also show heterogeneity between different tissues from the same tooth. The $\delta^{238}U$ and $\delta^{234}U_{sec}$ data of enameloid and dentine from 5 fossil shark teeth from two localities indicate the differences between tissue substrates (Fig. 5b). Generally, dentine samples have similar or lower $\delta^{238}U$ values than enameloid and $\delta^{234}U_{sec}$ values that deviate more from secular equilibrium. The magnitude of U isotope offsets between the enameloid and dentine varies among these samples ($\Delta_{enamel-dentine} = -0.04$–0.21 ‰).

3.3. O isotopes

The O isotope compositions of fossil shark teeth are presented in Table 1 and their relationships between the U isotope compositions are shown in Fig. 6. Compared to modern shark teeth, which show typical $\delta^{18}O_{PO4}$ values between 22 and 26 ‰ (mainly reflects the temperature and the O isotope composition of ambient water, Vennemann et al., 2001), enameloid $\delta^{18}O_{PO4}$ values in the fossil teeth studied here vary between 9.1 and 24.0 ‰ and define two main clusters. The Arctic shark teeth have lower $\delta^{18}O_{PO4}$ values (<19 ‰) and range of compositions (9.1–18.5 ‰). A correlation between $\delta^{238}U$ and $\delta^{18}O_{PO4}$ is not observed, while $\delta^{234}U_{sec}$ is positively correlated with $\delta^{18}O_{PO4}$. In contrast, samples from Peru and GOM have higher $\delta^{18}O_{PO4}$ (>19 ‰) and have a smaller range of compositions (19.2–24.0 ‰).

4. Discussion

4.1. Timing of U incorporation in shark teeth

Uranium concentrations are high in fossil shark teeth but negligible in modern teeth, indicating that U in fossil teeth derives from post-mortem incorporation. Uranium isotope records in fossil shark teeth are therefore not impacted by in-vivo factors (*i.e.*, lack vital effects), which could be an advantage for using shark teeth as a geochemical archive, in comparison to biological carbonates that can have variable vital effects (0–0.09 ‰, Chen et al., 2018b).

While the absence of vital effects is a strength of fossil shark teeth as a U isotope archive, postmortem acquisition of U means that burial conditions can considerably impact the degree to which tooth-hosted U
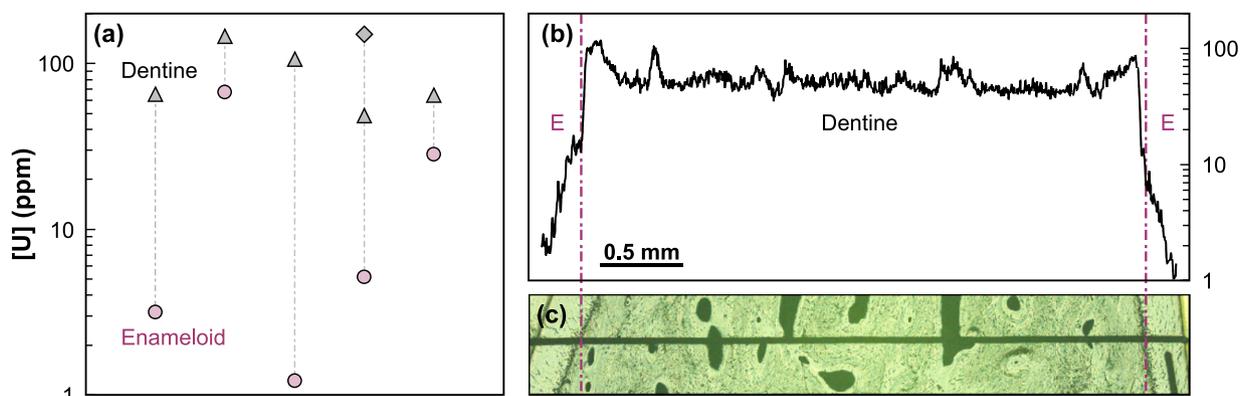
Fig. 4. U concentration trends across tissues. (a) Bulk U concentrations of enameloid and dentine from 5 fossil shark teeth. The dentine is shown in grey (triangle: crown, diamond: root) and enameloid samples are shown in pink circles. The vertical grey dash line connects the tissues from the same tooth. (b) Representative LA-ICPMS U concentration profile through the middle of a fossil tooth crown (2004–31-05). (c) Reflected light microscope image of the ablated cross section.
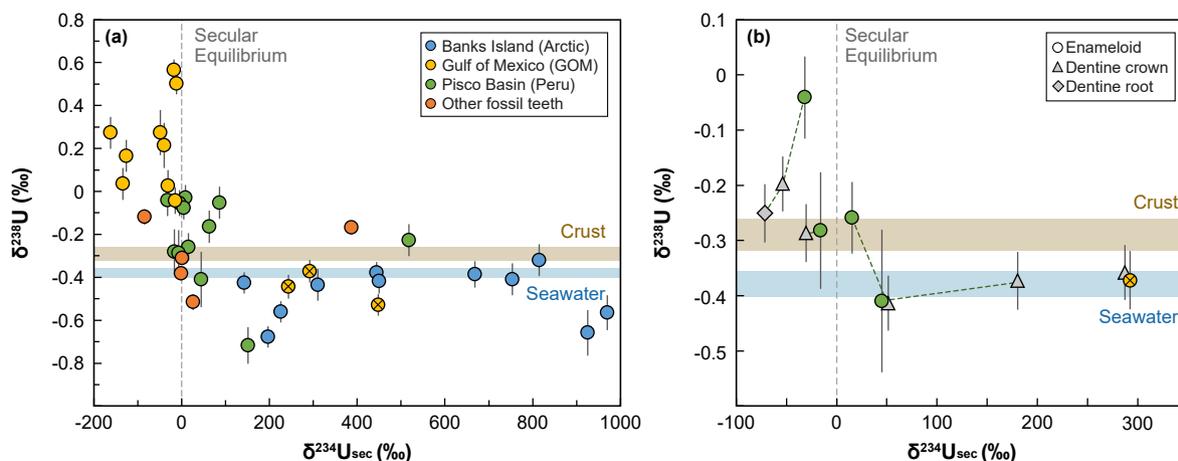

Fig. 5. $\delta^{238}U$ vs. $\delta^{234}U_{sec}$ in (a) the shark teeth enameloid from different localities, and (b) different tissues (*i.e.*, enameloid and dentine) in the same teeth. The color of enameloid symbols indicate localities, same as panel (a). Samples from the GOM are categorized into two groups based on their evolution history. Yellow $\otimes$ represents the first group with elevated $\delta^{234}U_{sec}$ values and $\delta^{238}U$ near modern seawater. Dashed lines connect different tissues from the same tooth. The brown and blue horizontal band show $\delta^{238}U$ of continental crust (-0.29 ± 0.03 ‰) and modern seawater (-0.379 ± 0.023 ‰) respectively (Tissot and Dauphas, 2015; Andersen et al., 2016; Kipp et al., 2022). The vertical grey dash line denotes the secular equilibrium $\delta^{234}U_{sec}$.
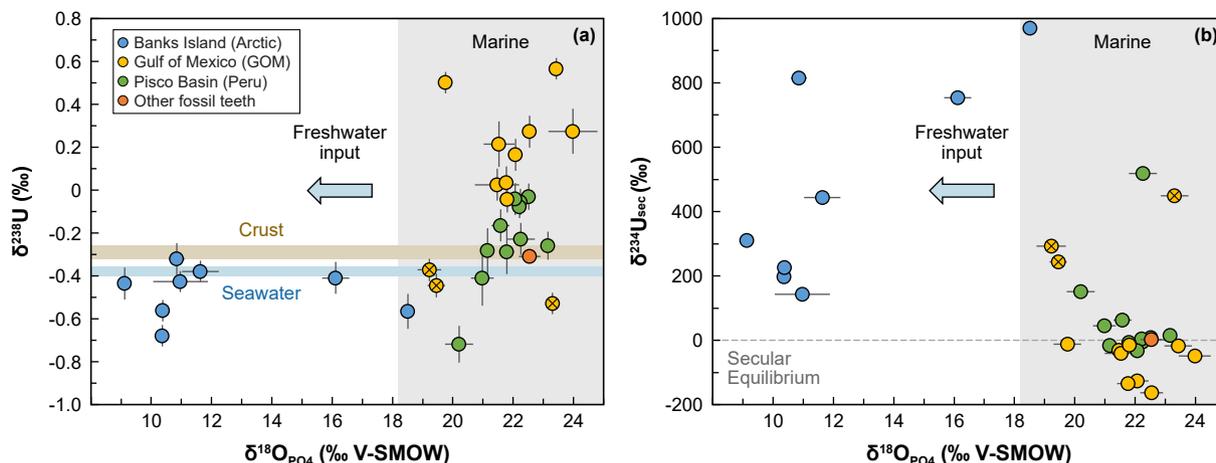
Fig. 6. (a) $\delta^{238}U$ vs. $\delta^{18}O_{PO4}$ and (b) $\delta^{234}U_{sec}$ vs. $\delta^{18}O_{PO4}$ in enameloid tissues of fossil shark teeth. Symbols as in Fig. 5. The vertical light grey band denotes the expected $\delta^{18}O_{PO4}$ range (Klug et al., 2010; Fischer et al., 2013) for marine sharks.

isotope signatures resemble those of primary seawater. Thus, for robust application of the U isotope redox proxy in fossil shark teeth, we need to first understand the timescale and mechanism of U uptake. Here, it is helpful to consider the uptake of not just U, but also other elements with similar behavior in biogenic apatite.

A disparity in concentration between modern and fossil teeth is in fact observed for a variety of trace elements (*e.g.,* U, Th and rare earth elements, REEs) in conodonts and fish teeth (Shaw and Wasserburg, 1985; Staudigel et al., 1985; Kohn et al., 1999; Martin and Haley, 2000; Vennemann et al., 2001; Trueman and Tuross, 2002; Trotter and Eggins, 2006), which may imply similar uptake timescale(s) and mechanism(s) for these elements. For example, Nd – one of the most extensively-studied systems – is thought to be rapidly incorporated into shark teeth with other REEs during the fossilization from apatite to hydroxy-fluorapatite, early in the burial process in surface sediments (Shaw and Wasserburg, 1985; Staudigel et al., 1985; Martin and Haley, 2000; Martin and Scher, 2004; Huck et al., 2016; Kim et al., 2020). This process is similar to U uptake models for mammal teeth, which predict that U incorporation would reach equilibrium on as short as ∼ kyr timescales (Pike and Hedges, 2001). The similarity in U and REE uptake in bio-apatite is supported by their strong co-variance in fossil teeth (Li et al., 2023). If true, early uptake of U into teeth could mean that U isotope signatures record early porewater conditions, with the signatures then preserved on geologic (Myr) timescales.

The timescales of U uptake in fossil teeth are also reflected by intra-sample spatial concentration patterns. For instance, we can consider diffusion-adsorption (DA) models, which are widely used to describe U uptake in teeth. These models state that U diffuses into the teeth as uranyl ion and then adsorbs onto the mineral surface (Millard and Hedges, 1996; Pike and Hedges, 2001). In these models, the spatial distribution of U in teeth is controlled by the diffusion and the partition coefficient of uranyl between aqueous fluids and apatite. The differing concentrations of U in enameloid and dentine (Kohn et al., 1999; Trotter and Eggins, 2006; Tütken et al., 2020; this study Fig. 4) can therefore be explained by their porosity difference. The higher porosity of dentine gives higher diffusion coefficient, resulting in higher U concentrations and a shorter time to reach equilibrium (Pike and Hedges, 2001).

Looking at the LA-ICPMS concentration profile across a representative shark tooth (2004–31-05, Fig. 4b), the relative history of U uptake can be reconstructed. First, higher [U] in dentine than enameloid reflects faster U diffusion into dentine and quicker accumulation of U from porewaters (*e.g.,* entering via the exposed root tissue). The U-rich dentine would then become a U source to the enameloid. Diffusion of U from dentine to enameloid is observed in the strong [U] gradient in enameloid, with concentrations steeply declining away from the junction with dentine. In other words, this process implies that formerly dentine-hosted U likely represents more of the enameloid U pool than the U that entered enameloid directly from porewater. In principle, the U concentration profiles in the teeth could provide a constraint on absolute timescales of U uptake, insofar as [U] is not homogenous in either enameloid or dentine, meaning that equilibrium was not achieved (or was recently disturbed). If equilibrium was not reached, it would imply a recrystallization timescale less than that required for [U] equilibration across tissues; in the models presented above, this timing could range from kyr to perhaps Myr timescales (Millard and Hedges, 1996; Pike and Hedges, 2001; Trueman and Tuross, 2002; Li et al., 2023). In practice, without knowledge of the sedimentary conditions (*e.g.,* [U] in sediments and porewater), it is difficult to precisely constrain the timescale of U incorporation with concentration data alone.

Beyond the early U uptake, our data also provide insights into whether recent U addition or loss occurred. Here, we use $\delta^{234}U_{sec}$ as a tracer of recent U mobility. An intermediate product of the ^{238}U decay chain, ^{234}U has a half-life ($t_{1/2}$) of ∼245 kyr (Cheng et al., 2013) and in a sample behaving as a closed-system the $^{234}U/^{238}U$ ratio will reach secular equilibrium after ∼2 Myr (*i.e.,* ∼8 half-lives). Given that the age of the fossil shark teeth investigated here are much older (all >5 Myr), if

they had behaved as closed systems following early diagenesis, their $\delta^{234}U_{sec}$ values should all be 0. However, most samples have $\delta^{234}U_{sec}$ values that deviate significantly from secular equilibrium (Fig. 5a), indicating that they experienced recent U open-system episodes. For the four out of five samples on which $\delta^{234}U_{sec}$ was measured in both enameloid and dentine, dentine tended to deviate more from secular equilibrium (Fig. 5b), implying that recent U mobilization is more pronounced in dentine than enameloid. This interpretation is consistent with the slow diffusion of U from dentine to enameloid tissues, and the idea that enameloid tissues are a more robust phase to target for paleo-environmental reconstructions (Kohn et al., 1999; Sharp et al., 2000; Becker et al., 2008; Thomas et al., 2011; McCormack et al., 2022).

In summary, U uptake in fossil shark teeth appears to have proceeded via rapid (kyr to Myr timescale) accumulation of U in the dentine followed by slow diffusion of U into enameloid tissues. Concentration gradients suggest that [U] did not reach equilibrium in the fossil teeth systems. Furthermore, $\delta^{234}U_{sec}$ variations suggest that recent U mobilization has occurred in the last 2 Myr. Collectively, these observations depict a complicated history of U uptake in fossil shark teeth.

4.2. Shark teeth do not uniquely record the seawater $\delta^{238}U$ composition

We now consider the ability of shark teeth to record ancient seawater U isotope ratios. The $\delta^{238}U$ values of shark teeth display considerable variability around the plausible seawater composition (Fig. 5), assuming that Cenozoic seawater was isotopically indistinguishable from modern seawater (Wang et al., 2016). Even allowing for moderate variation in seawater $\delta^{238}U$, many shark teeth display values exceeding those of the riverine input (>−0.3 ‰) (Andersen et al., 2016; Noordmann et al., 2016), which likely reflect diagenetic ^{238}U enrichment (*e.g.,* Bura-Nakić et al., 2020; Chen et al., 2018a; Clarkson et al., 2021a; del Rey et al., 2020; Hood et al., 2018; Romaniello et al., 2013; Tissot et al., 2018; White et al., 2018; Zhang et al., 2019). To first order, this means that for U isotopes, shark teeth do not directly preserve a snapshot of coeval seawater during the fossilization process.

If U isotopes in fossil shark teeth are not uniquely representative of the seawater composition, what are the processes that contribute to the observed isotopic variability? Diagenesis is known to significantly impact many geochemical proxies in sedimentary archives, including the $\delta^{238}U$ proxy in the most popular archives, carbonates and shales (Asael et al., 2013; Romaniello et al., 2013; Chen et al., 2018a; Phan et al., 2018; Tissot et al., 2018). The same is true for $\delta^{18}O$ values in conodonts and fish teeth (Iacumin et al., 1996; Kohn et al., 1999; Sharp et al., 2000; Zazzo et al., 2004b; Chen et al., 2015). Hence, it is likely that the U isotope compositions of the shark teeth studied here have strayed from the seawater value during diagenetic transformations. Below, we consider several syn- and post-depositional processes that may shape the U isotope composition of shark teeth (Fig. 7). These can be broken into four main categories: (1) detrital contamination, (2) isotope fractionation during U incorporation into the teeth, (3) assimilation of porewater U with isotope ratio deviating from that of seawater, and (4) recent U gain/loss.

4.2.1. Detrital contamination

Some of the U isotope variability observed in the shark teeth could be due to incorporation of detrital components. For instance, cavities can serve as reservoirs for detritus after the loss of basal body postmortem (Schmitz et al., 1991; Trotter and Eggins, 2006). Here we tracked detrital contributions to the tooth signatures with U/Th ratios (Figs. 8 and 9). Detrital inputs are characterized by high Th contents (*i.e.,* low U/Th ratios) and a crustal $\delta^{238}U$ value of −0.30 ± 0.04 ‰ (Tissot and Dauphas, 2015; Andersen et al., 2016). Previous work has shown that detrital inputs can modify both [U] and $\delta^{238}U$ in sedimentary archives (Asael et al., 2013; Noordmann et al., 2015; Lau et al., 2016; Tarhan et al., 2018; Kendall et al., 2020). The impact of detrital inputs on shark teeth has also been observed for other geochemical tracers (Elderfield
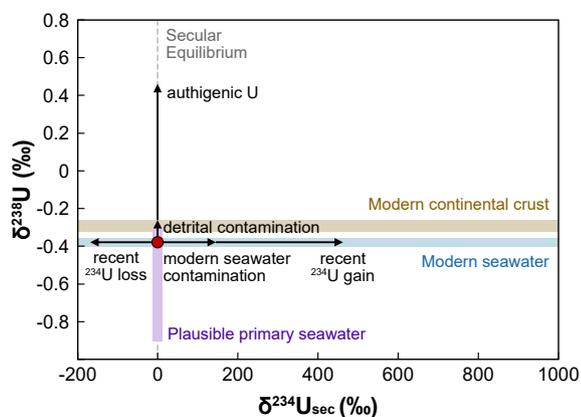
Fig. 7. Schematic impact of various processes on U isotope composition. The red circle represents the present archive values assuming preservation of primary seawater compositions and closed-system behavior since sample formation (*i.e.*, ^{234}U/^{238}U ratio at secular equilibrium). The light purple band indicates the plausible primary seawater δ^{238}U values (from −0.90 to −0.30 ‰) in the geological past, based on the model in (Kipp and Tissot, 2022). The brown and blue horizontal bands show δ^{238}U of continental crust (−0.29 ± 0.03 ‰) and modern seawater (−0.379 ± 0.023 ‰), respectively (Tissot and Dauphas, 2015; Andersen et al., 2016; Kipp et al., 2022), and the vertical grey dash line shows δ^{234}U$_{sec}$ value at secular equilibrium. For δ^{238}U, detrital contamination can only generate elevated δ^{238}U values up to the value of continental crust, while the authigenic input of reduced U can lead to larger magnitude of δ^{238}U. For δ^{234}U$_{sec}$, the incorporation of modern seawater can only lead to ^{234}U$_{sec}$ excess up to the modern seawater level (+145.55 ‰, Kipp et al., 2022), while recent (<2 Myr) ^{234}U gain (loss) relative to ^{238}U can result in larger δ^{234}U$_{sec}$ variability. The U isotope compositions of shark teeth typically reflected a combination of these processes.

and Pagett, 1986; Lécuyer et al., 2004; Kocsis et al., 2009; Ehret et al., 2012; Chen et al., 2015), suggesting it could be important for U as well. If detrital U is present in shark teeth, correlations between U isotope compositions and U/Th ratios would be expected, which would represent the mixing of authigenic and detrital components. The relationship between U isotope composition and U/Th does not define a unique relationship for all fossil shark teeth (Fig. 8). However, when considering each location independently, some correlations are observed, specifically in the δ^{238}U vs. U/Th diagram of GOM and the δ^{234}U$_{sec}$ vs. U/Th diagram of the Arctic (Fig. 9c, d). While these trends could suggest a control of detrital contamination, in neither case is detrital mixing able to explain trends in both δ^{238}U and δ^{234}U$_{sec}$. Furthermore, most of these teeth have far higher [U] (several to several hundred ppm) than detrital

material (2.7 ppm, Rudnick and Gao, 2014), meaning nuggets of detritus should only have a small impact on the bulk sample composition. Thus, we conclude that detrital contamination has a negligible impact on U isotopes in the fossil shark teeth studied here.

4.2.2. Isotopic fractionation during U incorporation into teeth

In theory, the uptake process itself could lead to isotope fractionation. Incorporation of U in teeth is thought to occur via diffusion of uranyl ions from surrounding water followed by adsorption on bioapatite (Millard and Hedges, 1996; Pike and Hedges, 2001). Since these processes do not involve a change in valence state, which is the mechanism generating the largest low-temperature U isotope fractionation in surface environments (Bigeleisen, 1996; Brown et al., 2018), the diffusion and adsorption are unlikely to be the cause of the large U isotopes variations observed in this study. Nevertheless, U adsorption on ironmanganese oxides is well-known to result in preferential incorporation of light U isotopes in the adsorbed phases, by ~0.20 ‰ (Brennecka et al., 2011; Wang et al., 2016). Assuming a similar isotopic fractionation during adsorption on apatite in the teeth could explain the lower δ^{238}U observed in some teeth (but not the higher δ^{238}U values).

Alternatively, uptake processes involving U reduction could result in significant U isotope fractionation. For instance, interaction between the organic matter in the teeth and the pore fluid could result in locally reducing conditions and U incorporation occurring via U reduction. In this case, the addition of authigenic U would manifest as a coincident increase in [U] and δ^{238}U. Here, such a [U] versus δ^{238}U correlation is observed at one site (GOM, Fig. 10c). These are among the most ^{238}U-enriched samples in the entire dataset, consistent with a role of U reduction in supplying extra U to the system. In summary, incorporation of authigenic reduced U is capable of generating the magnitude of observed isotopic fractionation.

4.2.3. Porewater U isotope ratios deviating from seawater

In another end-member scenario, the variations in δ^{238}U in shark teeth would not result from fractionation during U incorporation into the teeth, but simply record the composition of the surrounding porewaters. In this scenario, porewaters that start with a seawater δ^{238}U value could drift toward different compositions if U is added or removed with associated isotopic effects, and this altered composition could then become recorded in teeth upon U uptake.

The dominant process generating δ^{238}U variability in marine sediments is U(VI) reduction to U(IV) (*e.g.,* Stirling et al., 2007; Weyer et al., 2008). If this process were to occur in sediments hosting shark teeth, it would progressively decrease [U] and δ^{238}U in porewaters. There is perhaps evidence of this in the lower δ^{238}U values in the Arctic data
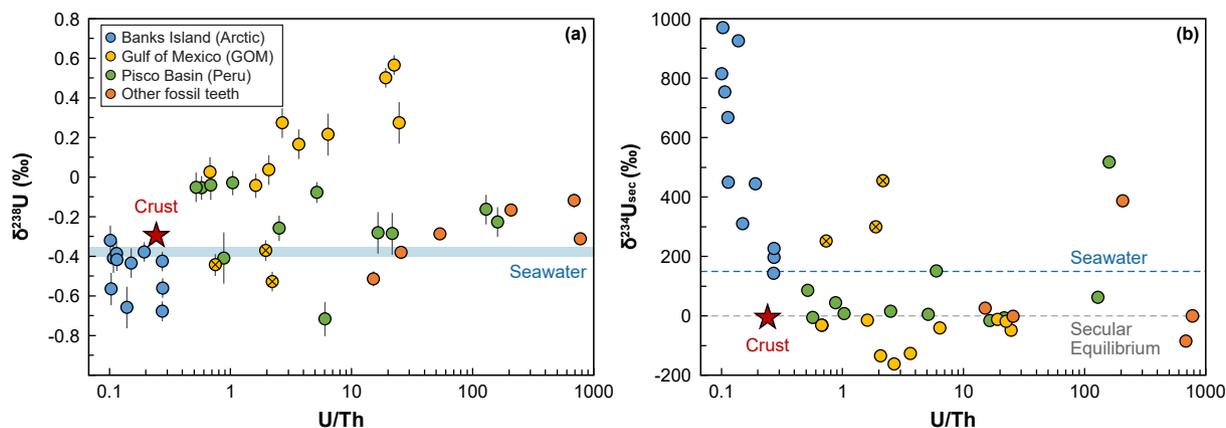

Fig. 8. (a) δ^{238}U vs. U/Th and (b) δ^{234}U$_{sec}$ vs. U/Th in enameloid tissues of fossil shark teeth. The red star represents the composition of continental crust, with δ^{238}U value of −0.29 ‰ (Tissot and Dauphas, 2015; Andersen et al., 2016), and U/Th ratio of 0.257 (Rudnick and Gao, 2014). The blue dash line represents the δ^{234}U$_{sec}$ value of modern seawater (+145.55 ‰, Kipp et al., 2022). Other symbols as in Fig. 5.
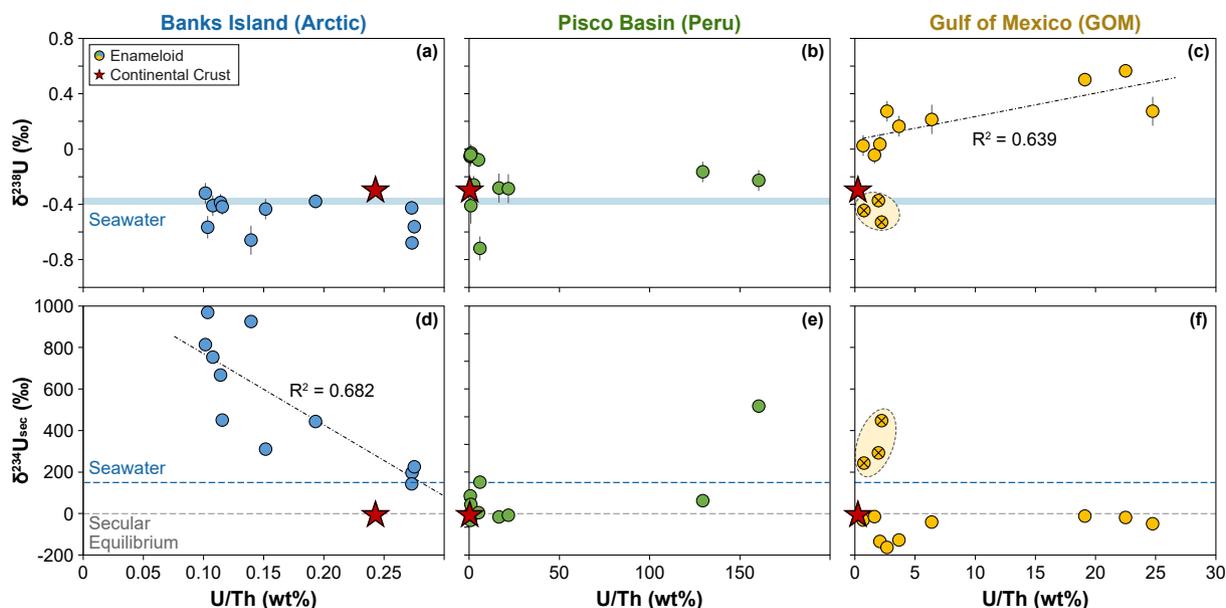
Fig. 9. U isotope trends vs. U/Th concentration ratios in enameloid tissues of fossil shark teeth. Symbols as in Fig. 8. The light yellow ellipses highlight the first group of fossil shark teeth from GOM.
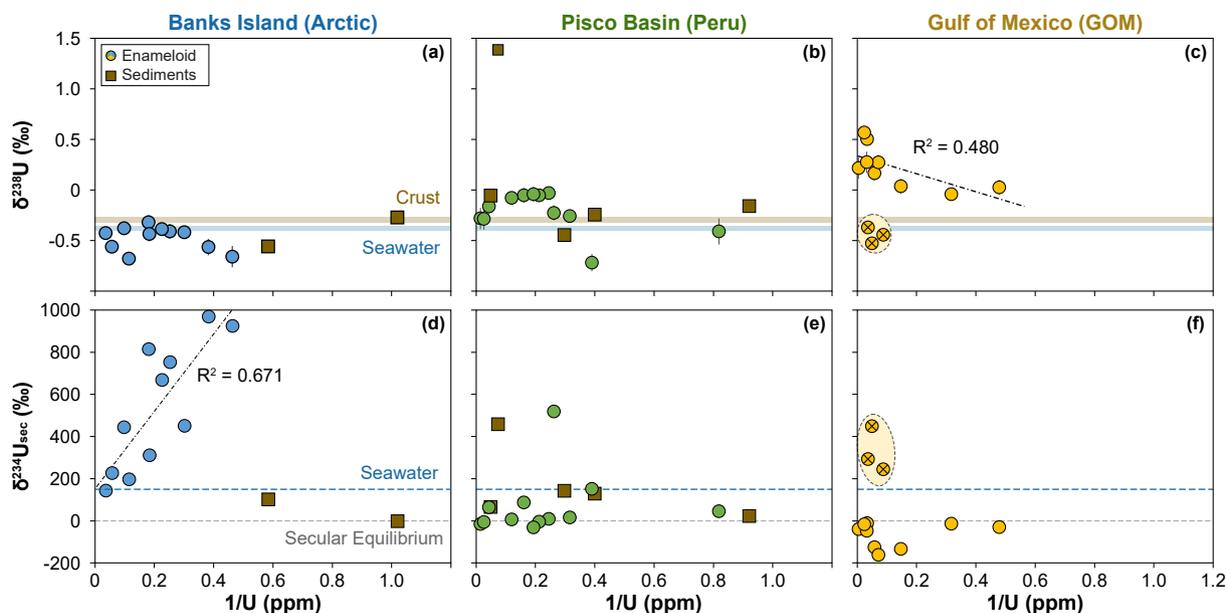

Fig. 10. U isotope vs. U concentration in sediments and the enameloid of fossil shark teeth. Symbols as in Fig. 5.

(Fig. 10a). Conversely, if U reduction occurred and sequestered isotopically heavy U(IV) in sediments, and the sediments were then flushed with oxidizing porewaters, a large release of ^{238}U-enriched U would occur, which could potentially become sequestered in shark teeth. The elevated δ^{238}U values in GOM data can support this possibility (Fig. 10c). These scenarios are not mutually exclusive, and it is quite possible that a given depositional environment oscillated between both conditions for multiple times before lithification.

To disambiguate between these possibilities, we can consider the δ^{238}U values of sediments hosting the fossil shark teeth. The first scenario, with isotopic distillation of porewaters due to U reduction, would predict low δ^{238}U in teeth and high δ^{238}U in sediments. The second scenario, with release of isotopically-modified authigenic U, would predict similar δ^{238}U in teeth and sediments (because sediments

supplied U to the teeth). In both the Arctic and Peru datasets, a similarity in sediments and teeth δ^{238}U values favors the latter scenario. The isotopically-fractionated sediments may have become enriched in U via reductive immobilization and subsequent interaction with oxidizing porewaters may have liberated some U, a fraction of which ultimately became sequestered in the shark teeth. Importantly, δ^{238}U signatures in these two localities have both higher and lower values than the continental crust, meaning that the U isotope signatures in shark teeth is not dominated by detrital U contamination. Besides the incorporation of porewater with low δ^{238}U values due to local reduction, U adsorption on ferromanganese oxides is another process that could explain lower than seawater δ^{238}U values. Absorbed U on Fe-Mn oxides is isotopically lighter than aqueous U by ~0.22 ‰ (Brennecka et al., 2011), which is comparable to the magnitude of δ^{238}U offsets observed in these samples.

This hypothesis is further supported by the elevated Fe and Mn concentrations in the enameloid of fossil teeth compared to modern teeth (**Table S2**, and Kohn et al., 1999).

Another way to alter pore fluid composition is to introduce meteoric fluids with isotopically-fractionated U (Polyak et al., 2023). Meteoric fluid can be identified using $\delta^{18}O$ values, since Rayleigh distillation depletes ^{18}O in rainfall, giving meteoritic fluid a lower $\delta^{18}O$ values than seawater (Dansgaard, 1964; LeGrande and Schmidt, 2006). In this view, the input of freshwater will lower $\delta^{18}O_{PO4}$ values in shark teeth (Kocsis et al., 2007; Klug et al., 2010; Fischer et al., 2013). If all fossil shark teeth are considered as a single group, no systematic correlations between U isotope compositions and $\delta^{18}O_{PO4}$ are observed (Fig. 6). However, at least in the Arctic, low $\delta^{18}O$ values point to freshwater input (Kim et al., 2014). Thus, while meteoric fluids may have played a role in shaping $\delta^{18}O$ patterns, it is an unlikely explanation for the large U isotope fractionations observed in these samples.

In summary, while meteoric diagenesis likely does not account for the observed trends, a contribution of sediment-hosted authigenic U to the tooth-hosted U pool could have generated much or all of the observed $\delta^{238}U$ variability.

4.2.4. U isotope fractionation during U gain/loss

The large range of $\delta^{234}U_{sec}$ values in shark teeth (Fig. 5) testifies to recent U mobilization (<2 Myr ago). If these shark teeth incorporated only modern seawater, they would record a $\delta^{234}U_{sec}$ value of +145.55 ‰ (Fig. 7, Chen et al., 1986; Andersen et al., 2010; Kipp et al., 2022). In contrast, the samples present ^{234}U excesses of up to ∼ +1000 ‰, reminiscent of the highly variable and elevated $\delta^{234}U_{sec}$ values observed in rivers, which can reach over +1000 ‰ (Chabaux et al., 2001, 2003; Robinson et al., 2004; Andersen et al., 2007, 2016). The same phenomenon responsible for the elevated $\delta^{234}U$ of rivers waters, alpha recoil, can readily explain the ^{234}U systematics of shark teeth. During alpha decay of ^{238}U, a fraction of the daughter nuclide ^{234}Th can be expelled as a result of the recoil effect into the surrounding porewater and rapidly decay into ^{234}U, leading to a ^{234}U excess at a few thousand permil scale (Henderson et al., 1999). The direct incorporation of porewater with ^{234}U excess can result in high $\delta^{234}U_{sec}$ values that are comparable to those measured in this study. On the other hand, alpha-recoil of the apatite-hosted U can explain the lower $\delta^{234}U_{sec}$ values observed in the samples. Indeed, the recoil-produced ^{234}U, even if not directly expelled from the mineral, can be preferentially mobilized out of damaged lattice site during aqueous leaching, compared to the lattice-bond ^{238}U (Kigoshi, 1971). Both U loss by leaching and/or alpha recoil

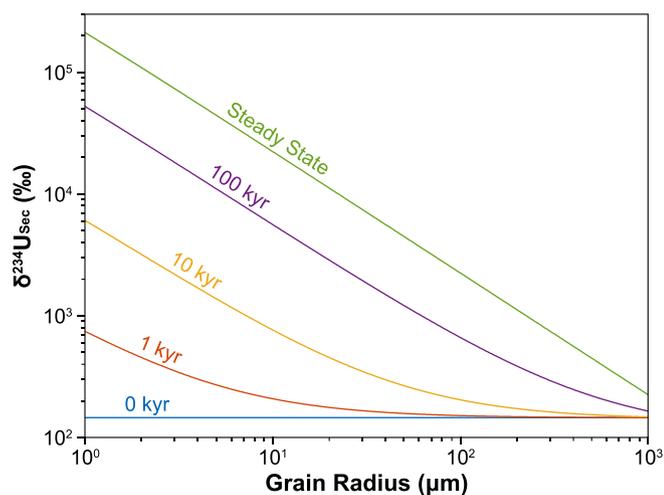**Fig. 11.** Predicted $\delta^{234}U_{sec}$ vs. grain radius in porewater-sediments system from the model in Henderson et al. (1999). The curve of steady state indicates the upper limit of $\delta^{234}U_{sec}$ can be generated in porewater system.

would be consistent with the [U] profile in Fig. 4. To assess the impact of alpha recoil on ^{234}U excesses, the $\delta^{234}U_{sec}$ of porewater is plotted against the grain radius (Fig. 11) using the established model in Henderson et al. (1999). The maximum ^{234}U excesses that can be generated by alpha recoil process are larger than the observed $\delta^{234}U_{sec}$ values in shark teeth, which strengthen the interpretation that alpha-recoil in porewater can lead to the ^{234}U excesses in shark teeth.

We note that while alpha recoil can readily account for the variations of $\delta^{234}U_{sec}$ in shark teeth, both the riverine and modern seawater inputs may also contribute to the ^{234}U budget in the samples. Given that these mechanisms are not necessarily correlated to other proxies (*i.e.*, [U] and $\delta^{238}U$), we are not able to disentangle their relative impacts on the compositions of the samples.

4.3. Evaluation of U uptake and isotopic alteration history at each site

Shark teeth from the 3 localities in this study have distinct characteristics in the variability of $\delta^{238}U$ and $\delta^{234}U_{sec}$ as well as their relationships with diagenetic tracers, indicating that U uptake and isotopic fractionation is controlled by local environmental conditions. Here, we look at the history of U incorporation and isotopic alteration at each site, considering the implications for the use of shark teeth as an archive of ancient seawater U isotope ratios.

4.3.1. Banks Island (Arctic)

In the Arctic shark teeth, the range of $\delta^{238}U$ is relatively limited around the modern seawater value (−0.48 ± 0.12 ‰, ± 1 SD). On the other hand, $\delta^{234}U_{sec}$ values are highly variable, and all exhibit ^{234}U excess, most likely caused by the alpha-recoil in the porewater system. Correlations of $\delta^{234}U_{sec}$ vs. $\delta^{18}O$, U/Th, and 1/U are observed (Fig. 6b, Fig. 9d, Fig. 10d), and provide clues to understand the geological processes that controlled the U isotope fractionation in this location. Shark teeth from the Eocene Arctic are significantly depleted in ^{18}O relative to the other locations, reflecting freshwater inputs into the Arctic during the early Eocene (Kim et al., 2014), such as meteoric water and rivers. In this framework, the low [U] and high $\delta^{234}U_{sec}$ values of river water (Chabaux et al., 2001, 2003; Robinson et al., 2004; Andersen et al., 2007, 2016), are consistent with initial uptake of riverine U in the teeth. The estimated salinity of northern Banks Island during the Eocene is 12.7 PSU (Kim et al., 2014), which is substantially lower than the central Arctic Ocean during the Eocene (21–25 PSU, Waddell and Moore, 2008), and the modern Arctic Ocean (32–35 PSU, Boyer et al., 2009), implying the U mass balance in the Banks Island region was not dominated by open ocean. Subsequent uptake of seawater U in the teeth would then readily explain the positive correlation between $\delta^{234}U_{sec}$ and 1/U (R^2 = 0.671, Fig. 10d), and the convergence towards a seawater like $\delta^{234}U_{sec}$ value in the samples with the highest [U].

The limited $\delta^{238}U$ variability around a seawater-like value in the Arctic teeth samples could reflect either (i) preservation of the original $\delta^{238}U$ of seawater during the early Eocene with a similar composition as modern seawater or (ii) incorporation of U from modern seawater during recent reworking. For the most U-rich samples, the evidence points to a predominant control of the U budget by recent U addition (*i.e.*, seawater-like $\delta^{238}U$ and $\delta^{234}U_{sec}$, and a clear correlation between $\delta^{234}U_{sec}$ and 1/U). In the most U-depleted samples, the elevated $\delta^{234}U_{sec}$ values preclude addition of seawater U in the last 2 Myr, but the available information is insufficient to determine if the $\delta^{238}U$ values in these samples preserve the seawater composition at the time of burial (Eocene), or a more recent U addition (prior to 2 Myr ago).

4.3.2. Gulf of Mexico (GOM)

Based on their U isotope compositions, Eocene shark teeth from GOM can be grouped into subsets that are likely to have had different evolution histories. The first group (yellow ⊗), similar to the Arctic samples, display elevated $\delta^{234}U_{sec}$ values (>+200 ‰), $\delta^{238}U$ around the modern seawater value and higher Fe and Mn contents, which are most readily

explained by exchange with pore fluids and incorporation of contemporary seawater. The second group shows $\delta^{234}U_{sec}$ near secular equilibrium and elevated $\delta^{238}U$ values. Limited deviations of $\delta^{234}U_{sec}$ from secular equilibrium imply that these teeth did not experience recent resetting, Examination of a $\delta^{238}U$ vs. U/Th plot (Fig. 9c) shows that the spread in $\delta^{238}U$ of the samples is not primarily controlled by incorporation of a detrital component. Since large $\delta^{238}U$ variations reflecting globally expanded marine anoxia/oxygenation were not observed during the Cenozoic (Goto et al., 2014; Wang et al., 2016; Gothmann et al., 2019), the higher $\delta^{238}U$ values of the second group from GOM are best explained by the locally reducing conditions driving U isotope fractionation during early U uptake in the samples.

4.3.3. Pisco Basin (Peru)

Most Miocene shark teeth from Peru show moderate enrichment in ^{238}U relative to the modern seawater (<+0.4 ‰). This range of $\delta^{238}U$ values is similar to the one observed in the surrounding sediments, suggesting that the addition of reduced isotopically heavy U may contribute to the $\delta^{238}U$ observed in shark teeth. The lack of correlation between $\delta^{238}U$ and 1/[U] reveals however a more complicated U evolution history than for the samples from GOM, whereby the addition of heavy U only influenced but did not dominate the U isotope signals in shark teeth. It is notable that one sediment sample has an extremely high $\delta^{238}U$ value (+1.38 ‰), which is much higher than the $\delta^{238}U$ signatures of the sediments from the representative anoxic setting – the Black Sea (Montoya-Pino et al., 2010; Andersen et al., 2014; Rolison et al., 2017; Brüske et al., 2020). This observation reflects that ^{238}U can be preferentially scavenged into sediments under local reducing conditions, which also results in a decrease in the seawater $\delta^{238}U$ value. The incorporation of such seawater can explain why some shark teeth from Peru have $\delta^{238}U$ values much lower than modern seawater. Sediments from the Pisco Basin show large variations in $\delta^{238}U$ values (−0.45–+1.38 ‰), indicating potential spatial–temporal changes in the redox state of the local burial environment. In most of the samples, the secular equilibrium $\delta^{234}U_{sec}$ values indicate that the incorporation of U happened more than ~2 Myr ago. In a small subset of the samples, modern seawater $\delta^{234}U_{sec}$ values, indicating the recent exchange with the seawater.

4.4. Outlook for U isotopes in fossil fish teeth as a paleoredox proxy

Our results demonstrate that shark teeth were affected by post-depositional processes, which modified their primary U isotope signatures to varying degrees. Given that such sample alteration is common in paleoenvironmental reconstructions, and keeping in mind the relatively small data set for fossil shark teeth, we conduct a preliminary evaluation of the robustness of the teeth paleoredox proxy against other widely used archives, including corals (Romaniello et al., 2013; Chen et al., 2018a, b; Gothmann et al., 2019; Kipp et al., 2022), marine carbonate sediments (Romaniello et al., 2013; Noordmann et al., 2016; Chen et al., 2018a, 2021, 2022; Bura-Nakić et al., 2018; Tissot et al., 2018; Clarkson et al., 2021b; Lau et al., 2022; Martin et al., 2023; Zhang et al., 2023), and ferromanganese crusts (Goto et al., 2014; Wang et al., 2016).

The spread of U isotopes in Cenozoic samples from these 4 types of archives are shown in Fig. 12 and Table 2. Previous studies suggested indistinguishable seawater $\delta^{238}U$ throughout the Cenozoic (Wang et al., 2016; Gothmann et al., 2019). If correct, this means that a faithful U isotope archive preserving the primary seawater signature should have $\delta^{238}U$ resembling modern seawater and $\delta^{234}U_{sec}$ near secular equilibrium. As is well-known (e.g., Kipp et al., 2022), corals can preserve superbly the original seawater signals, showing very limited variations in both $\delta^{238}U$ and $\delta^{234}U_{sec}$, as well as $\delta^{238}U$ values concentrated around the modern seawater composition. Iron-manganese crusts also show limited variations in $\delta^{238}U$ centered around the seawater value, but serious doubts have been raised regarding the primary nature of these signatures (Li and Tissot, 2023). Indeed, Fe-Mn crusts have $^{234}U/^{238}U$ ratios widely out of secular equilibrium, and, in many cases, offset towards the modern seawater value, suggesting recent U exchange and equilibration between the Fe-Mn crusts and seawater. Compared to corals, fossil shark teeth and carbonates display much larger U isotope variations, indicating a more complicated U incorporation history, and thus redox inferences that are bound to be more uncertain.

The limited data on fossil shark teeth samples prevents a proper statistical analysis. Taken at face value, fossil shark teeth have an average $\delta^{238}U$ value (−0.22 ‰) closer to modern seawater (−0.379 ‰) than carbonate sediments, which are biased towards higher values (−0.16 ‰, as noted in Chen et al., 2018a; Tissot et al., 2018). On the
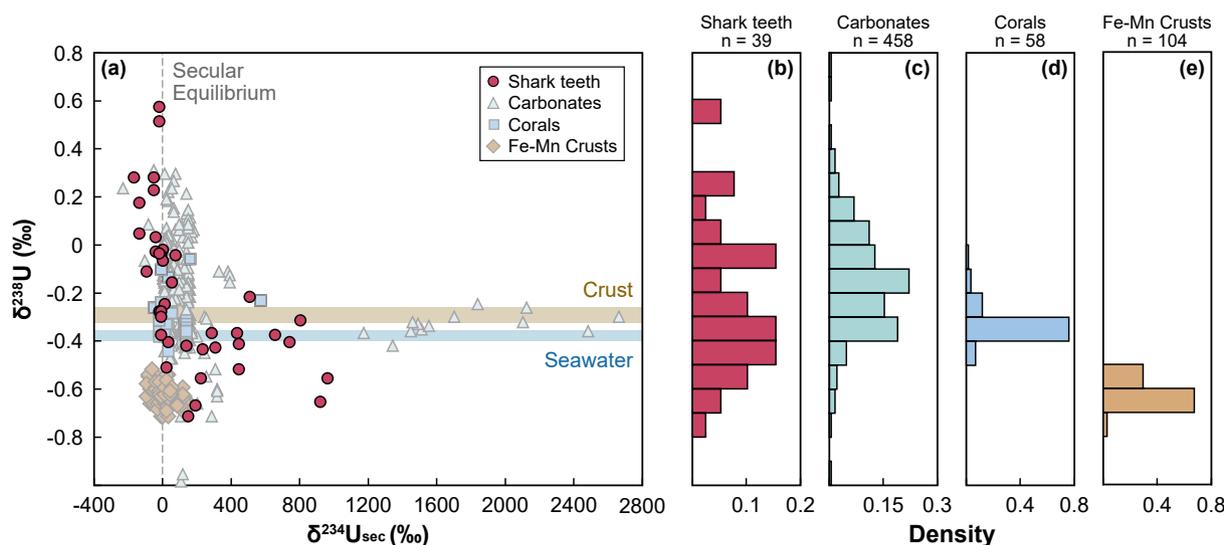

Fig. 12. U isotopes variations in Cenozoic (up to 66 Ma) shark teeth and various archives used for paleoredox reconstructions. (a) $\delta^{238}U$ vs. $\delta^{234}U_{sec}$ (b)-(e) Histogram of $\delta^{238}U$ in fossil shark teeth (this study), sedimentary carbonates (Romaniello et al., 2013; Noordmann et al., 2016; Chen et al., 2018a, 2021, 2022; Bura-Nakić et al., 2018; Tissot et al., 2018; Clarkson et al., 2021b; Lau et al., 2022; Martin et al., 2023; Zhang et al., 2023), coral (Romaniello et al., 2013; Chen et al., 2018a, b; Gothmann et al., 2019; Kipp et al., 2022), Fe-Mn crust (Goto et al., 2014; Wang et al., 2016). Shark teeth show larger deviations in both $\delta^{238}U$ (away from modern seawater) and $\delta^{234}U_{sec}$ (away from secular equilibrium) than Fe-Mn crusts and fossil corals, as well as slightly smaller deviations than carbonates, suggesting that diagenesis, recent U loss/uptake and/or intra-sample U diffusion leads to large offsets between tooth-hosted U isotope ratios and those of coeval seawater. In panel (a), only data for which both $\delta^{238}U$ and $\delta^{234}U_{sec}$ are available are shown, while the full dataset is included in panel (b)-(e).

Table 2
Summary of U isotopes in paleoredox archives in Cenozoic (up to 66 Ma): shark teeth (this study), marine carbonate sediments (Romaniello et al., 2013; Noordmann et al., 2016; Chen et al., 2018a, 2021, 2022; Bura-Nakić et al., 2018; Tissot et al., 2018; Clarkson et al., 2021b; Lau et al., 2022; Zhang et al., 2023), coral (Romaniello et al., 2013; Chen et al., 2018a, b; Gothmann et al., 2019; Kipp et al., 2022), Fe-Mn crust (Goto et al., 2014; Wang et al., 2016).

Sample Type	δ^{238}U					δ^{234}U$_{sec}$				
	min	max	mean	±SD	n	min	max	mean	±SD	n
Shark Teeth	−0.72	0.57	−0.22	0.31	39	−162.1	969.7	181.5	304.5	39
Carbonates	−0.98	0.71	−0.16	0.22	458	−234.0	2669.0	150.9	357.8	310
Fe-Mn Crust	−0.71	−0.52	−0.63	0.04	104	−95.6	144.7	10.8	63.8	104
Coral	−0.45	−0.07	−0.34	0.07	58	−41.0	580.0	112.4	95.4	46

other hand, the fossil shark teeth data display slightly larger δ^{238}U variations (±0.31 ‰, 1SD) compared to carbonates (±0.22 ‰, 1SD). While the performance of fossil shark teeth as recorder of seawater U isotope composition can appear to roughly match that of carbonates, we emphasize that this conclusion is only a first-order assessment and is likely to be biased by (i) the different sample sizes (n_{shark_teeth} = 39, n_{carb_sed} = 458), and (ii) the clear evidence for recent addition of seawater U in the Arctic samples. Furthermore, diagenetic alterations are common in fossil shark teeth (*e.g.,* Toyoda and Tokonami, 1990; Tütken et al., 2011), and the local scale diagenesis can be unique for each investigated location, complicating inferences of global anoxia with this archive. A full assessment of the potential of U isotopes in fossil shark teeth as a paleoredox proxy will benefit from future work that (i) explore geological settings less prone to diagenetic overprinting (*e.g.,* pelagic open ocean), (ii) use prescreening of well-preserved samples (*e. g.,* appearance and in-situ [U] profiles), and (iii) implement diagenetic and/or detrital corrections (*e.g.,* δ^{18}O, Mn/Sr/Fe contents, U/Th, Mn/Sr, Mg/Ca, Sr/Ca, and TOC) to understand if such methods can reliably avoid the pitfalls associated with diagenetic overprints. Based on the current dataset, we provisionally conclude that shark teeth might have the potential to become a complementary archive for the U proxy, but do not have advantages over carbonate sediments and other more established archives.

5. Conclusion

The potential of bioapatite as a novel archive of past seawater δ^{238}U values was tested using fossil shark teeth from three localities (Arctic, GOM, and Peru) and ranging in age from early Eocene to the Miocene. Uranium concentrations in modern and fossil shark teeth differ significantly. Uranium contents are negligible in modern shark teeth (<1 ppb) but substantially higher and more variable in fossil samples (a few to a few hundred ppm), demonstrating that U was incorporated into shark teeth postmortem during burial. Fossil shark teeth δ^{238}U values range from −0.72 to +0.57 ‰, which is comparable to the variability observed in marine carbonate sediments. The U isotope composition of fossil shark teeth is influenced by local redox conditions and depositional environments. The impacts of these parameters notably complicate the interpretation of U isotope data in shark teeth. For future applications of δ^{238}U in shark teeth as a paleoredox proxy, screening and correction methods are recommended to overcome the effects of such secondary processes.

Data availability

Data are available through CaltechDATA at https://doi.org/10.22002/xe7v7-c1r13.

Declaration of competing interest

The authors declare that they have no known competing financial interests or personal relationships that could have appeared to influence the work reported in this paper.

Appendix A. Supplementary material

Supplementary material to this article can be found online at https://doi.org/10.1016/j.gca.2023.11.034.

References

Andersen, M.B., Stirling, C.H., Porcelli, D., Halliday, A.N., Andersson, P.S., Baskaran, M., 2007. The tracing of riverine U in Arctic seawater with very precise ^{234}U/^{238}U measurements. Earth Planet. Sci. Lett. 259, 171–185.

Andersen, M.B., Stirling, C.H., Zimmermann, B., Halliday, A.N., 2010. Precise determination of the open ocean ^{234}U/^{238}U composition. Geochemistry, Geophys. Geosystems 11 (12).

Andersen, M.B., Romaniello, S., Vance, D., Little, S.H., Herdman, R., Lyons, T.W., 2014. A modern framework for the interpretation of ^{238}U/^{235}U in studies of ancient ocean redox. Earth Planet. Sci. Lett. 400, 184–194.

Andersen, M.B., Vance, D., Morford, J.L., Bura-Nakić, E., Breitenbach, S.F.M., Och, L., 2016. Closing in on the marine ^{238}U/^{235}U budget. Chem. Geol. 420, 11–22.

Andersen, M.B., Stirling, C.H., Weyer, S., 2017. Uranium Isotope Fractionation. Rev. Mineral. Geochemistry 82, 799–850.

Asael, D., Tissot, F.L.H., Reinhard, C.T., Rouxel, O., Dauphas, N., Lyons, T.W., Ponzevera, E., Liorzou, C., Chéron, S., 2013. Coupled molybdenum, iron and uranium stable isotopes as oceanic paleoredox proxies during the Paleoproterozoic Shunga Event. Chem. Geol. 362, 193–210.

Barrat, J.A., Taylor, R.N., André, J.P., Nesbitt, R.W., Lecuyer, C., 2000. Strontium isotopes in biogenic phosphates from a Neogene marine formation: Implications for palaeoseawater studies. Chem. Geol. 168, 325–332.

Becker, M.A., Seidemann, D.E., Chamberlain, J.A., Buhl, D., Slattery, W., 2008. Strontium isotopic signatures in the enameloid and dentine of upper Cretaceous shark teeth from western Alabama: Paleoecologic and geochronologic implications. Palaeogeogr. Palaeoclimatol. Palaeoecol. 264, 188–194.

Bigeleisen, J., 1996. Nuclear size and shape effects in chemical reactions. Isotope chemistry of the heavy elements. J. Am. Chem. Soc. 118, 3676–3680.

Bosio, G., Malinverno, E., Collareta, A., Di Celma, C., Gioncada, A., Parente, M., Berra, F., Marx, F.G., Vertino, A., Urbina, M., Bianucci, G., 2020. Strontium Isotope Stratigraphy and the thermophilic fossil fauna from the middle Miocene of the East Pisco Basin (Peru). J. South Am. Earth Sci. 97.

Botella, H., Valenzuela-Ríos, J.I., Martínez-Perez, C., 2009. Tooth replacement rates in early chondrichthyans: A qualitative approach. Lethaia 42, 365–376.

Boyer, T.P., Antonov, J.I., Baranova, O.K., Garcia, H.E., Johnson, D.R., Mishonov, A. V, O'Brien, T.D., Seidov, D., Smolyar, I., Zweng, M.M., 2009. World ocean database 2009. in Levitus, S., ed., NOAA Atlas NESDIS 66: Washington, D.C., U.S. Government Printing Office, 216 p.

Brennecka, G.A., Wasylenki, L.E., Bargar, J.R., Weyer, S., Anbar, A.D., 2011. Uranium isotope fractionation during adsorption to Mn-oxyhydroxides. Environ. Sci. Technol. 45, 1370–1375.

Broecker, W.S. and Peng, T.H., 1982. Tracers in the Sea (Vol. 690). Palisades, New York: Lamont-Doherty Geological Observatory, Columbia University.

Brown, S.T., Basu, A., Ding, X., Christensen, J.N., DePaolo, D.J., 2018. Uranium isotope fractionation by abiotic reductive precipitation. Proc. Natl. Acad. Sci. U. S. A. 115, 8688–8693.

Brüske, A., Weyer, S., Zhao, M.Y., Planavsky, N.J., Wegwerth, A., Neubert, N., Dellwig, O., Lau, K.V., Lyons, T.W., 2020. Correlated molybdenum and uranium isotope signatures in modern anoxic sediments: Implications for their use as paleo-redox proxy. Geochim. Cosmochim. Acta 270, 449–474.

Bura-Nakić, E., Andersen, M.B., Archer, C., de Souza, G.F., Marguš, M., Vance, D., 2018. Coupled Mo-U abundances and isotopes in a small marine euxinic basin: Constraints on processes in euxinic basins. Geochim. Cosmochim. Acta 222, 212–229.

Bura-Nakić, E., Sondi, I., Mikac, N., Andersen, M.B., 2020. Investigating the molybdenum and uranium redox proxies in a modern shallow anoxic carbonate rich marine sediment setting of the Malo Jezero (Mljet Lakes, Adriatic Sea). Chem. Geol. 533, 119441.

Chabaux, F., Riotte, J., Clauer, N., France-Lanord, C., 2001. Isotopic tracing of the dissolved U fluxes of Himalayan rivers: Implications for present and past U budgets of the Ganges-Brahmaputra system. Geochim. Cosmochim. Acta 65, 3201–3217.

Chabaux, F., Riotte, J., Dequincey, O., 2003. U-Th-Ra fractionation during weathering and river transport. Uranium-Series Geochemistry 52, 533–576.

Chen, J.H., Lawrence Edwards, R., Wasserburg, G.J., 1986. ^{238}U, ^{234}U and ^{232}Th in seawater. Earth Planet. Sci. Lett. 80, 241–251.

Chen, J., Algeo, T.J., Zhao, L., Chen, Z.Q., Cao, L., Zhang, L., Li, Y., 2015. Diagenetic uptake of rare earth elements by bioapatite, with an example from Lower Triassic conodonts of South China. Earth-Science Rev. 149, 181–202.

Chen, X., Romaniello, S.J., Herrmann, A.D., Wasylenki, L.E., Anbar, A.D., 2016. Uranium isotope fractionation during coprecipitation with aragonite and calcite. Geochim. Cosmochim. Acta 188, 189–207.

Chen, X., Romaniello, S.J., Herrmann, A.D., Hardisty, D., Gill, B.C., Anbar, A.D., 2018a. Diagenetic effects on uranium isotope fractionation in carbonate sediments from the Bahamas. Geochim. Cosmochim. Acta 237, 294–311.

Chen, X., Romaniello, S.J., Herrmann, A.D., Samankassou, E., Anbar, A.D., 2018b. Biological effects on uranium isotope fractionation (^{238}U/^{235}U) in primary biogenic carbonates. Geochim. Cosmochim. Acta 240, 1–10.

Chen, X., Romaniello, S.J., McCormick, M., Sherry, A., Havig, J.R., Zheng, W., Anbar, A. D., 2021. Anoxic depositional overprinting of ^{238}U/^{235}U in calcite: When do carbonates tell black shale tales? Geology 49, 1193–1197.

Chen, X., Robinson, S.A., Romaniello, S.J., Anbar, A.D., 2022. ^{238}U/^{235}U in calcite is more susceptible to carbonate diagenesis. Geochim. Cosmochim. Acta 326, 273–287.

Cheng, H., Lawrence Edwards, R., Shen, C.-C., Polyak, V.J., Asmerom, Y., Woodhead, J., Hellstrom, J., Wang, Y., Kong, X., Spötl, C., Wang, X., Calvin Alexander, E., 2013. Improvements in ^{230}Th dating, ^{230}Th and ^{234}U half-life values, and U-Th isotopic measurements by multi-collector inductively coupled plasma mass spectrometry. Earth Planet. Sci. Lett. 371–372, 82–91.

Clarkson, M.O., Hennekam, R., Sweere, T.C., Andersen, M.B., Reichart, G.J., Vance, D., 2021a. Carbonate associated uranium isotopes as a novel local redox indicator in oxidatively disturbed reducing sediments. Geochim. Cosmochim. Acta 311, 12–28.

Clarkson, M.O., Lenton, T.M., Andersen, M.B., Bagard, M.L., Dickson, A.J., Vance, D., 2021b. Upper limits on the extent of seafloor anoxia during the PETM from uranium isotopes. Nat. Commun. 12, 1–9.

Dansgaard, W., 1964. Stable isotopes in precipitation. Tellus 16, 436–468.

del Rey, Á., Havsteen, J.C., Bizzarro, M., Dahl, T.W., 2020. Untangling the diagenetic history of uranium isotopes in marine carbonates: A case study tracing the δ^{238}U composition of late Silurian oceans using calcitic brachiopod shells. Geochim. Cosmochim. Acta 287, 93–110.

Dera, G., Pucéat, E., Pellenard, P., Neige, P., Delsate, D., Joachimski, M.M., Reisberg, L., Martinez, M., 2009. Water mass exchange and variations in seawater temperature in the NW Tethys during the Early Jurassic: Evidence from neodymium and oxygen isotopes of fish teeth and belemnites. Earth Planet. Sci. Lett. 286, 198–207.

Dunk, R.M., Mills, R.A., Jenkins, W.J., 2002. A reevaluation of the oceanic uranium budget for the Holocene. Chem. Geol. 190, 45–67.

Ehret, D.J., Macfadden, B.J., Jones, D.S., Devries, T.J., Foster, D.A., Salas-Gismondi, R., 2012. Origin of the white shark *Carcharodon* (Lamniformes: Lamnidae) based on recalibration of the Upper Neogene Pisco Formation of Peru. Palaeontology 55, 1139–1153.

Elderfield, H., Pagett, R., 1986. Rare earth elements in ichthyoliths: Variations with redox conditions and depositional environment. Sci. Total Environ. 49, 175–197.

Enax, J., Prymak, O., Raabe, D., Epple, M., 2012. Structure, composition, and mechanical properties of shark teeth. J. Struct. Biol. 178, 290–299.

Fischer, J., Voigt, S., Franz, M., Schneider, J.W., Joachimski, M.M., Tichomirowa, M., Götze, J., Furrer, H., 2012. Palaeoenvironments of the late Triassic Rhaetian Sea: Implications from oxygen and strontium isotopes of hybodont shark teeth. Palaeogeogr. Palaeoclimatol. Palaeoecol. 353–355, 60–72.

Fischer, J., Schneider, J.W., Voigt, S., Joachimski, M.M., Tichomirowa, M., Tütken, T., Götze, J., Berner, U., 2013. Oxygen and strontium isotopes from fossil shark teeth: Environmental and ecological implications for Late Palaeozoic European basins. Chem. Geol. 342, 44–62.

Ginter, M., Hampe, O., Duffin, C.J., 2010. Chondrichthyes: Paleozoic Elasmobranchii: Teeth. Dr. Friedrich Pfeil.

Gothmann, A.M., Higgins, J.A., Adkins, J.F., Broecker, W., Farley, K.A., McKeon, R., Stolarski, J., Planavsky, N., Wang, X., Bender, M.L., 2019. A Cenozoic record of seawater uranium in fossil corals. Geochim. Cosmochim. Acta 250, 173–190.

Goto, K.T., Anbar, A.D., Gordon, G.W., Romaniello, S.J., Shimoda, G., Takaya, Y., Tokumaru, A., Nozaki, T., Suzuki, K., Machida, S., Hanyu, T., Usui, A., 2014. Uranium isotope systematics of ferromanganese crusts in the Pacific Ocean: Implications for the marine ^{238}U/^{235}U isotope system. Geochim. Cosmochim. Acta 146, 43–58.

Hättig, K., Stevens, K., Thies, D., Schweigert, G., Mutterlose, J., 2019. Evaluation of shark tooth diagenesis-screening methods and the application of their stable oxygen isotope data for palaeoenvironmental reconstructions. J. Geol. Soc. London. 176, 482–491.

Henderson, G.M., Slowey, N.C., Haddad, G.A., 1999. Fluid flow through carbonate platforms: Constraints from ^{234}U/^{238}U and Cl⁻ in Bahamas pore-waters. Earth Planet. Sci. Lett. 169, 99–111.

Hood, A. V. S., Planavsky, N.J., Wallace, M.W., Wang, X., 2018. The effects of diagenesis on geochemical paleoredox proxies in sedimentary carbonates. Geochim. Cosmochim. Acta 232, 265–287.

Huck, C.E., van de Flierdt, T., Jiménez-Espejo, F.J., Bohaty, S.M., Röhl, U., Hammond, S. J., 2016. Robustness of fossil fish teeth for seawater neodymium isotope reconstructions under variable redox conditions in an ancient shallow marine setting. Geochemistry. Geophys. Geosystems 17, 679–698.

Iacumin, P., Bocherens, H., Mariotti, A., Longinelli, A., 1996. Oxygen isotope analyses of co-existing carbonate and phosphate in biogenic apatite: A way to monitor diagenetic alteration of bone phosphate? Earth Planet. Sci. Lett. 142, 1–6.

Kane, J.S., 1998. A history of the development and certification of NIST glass SRMs 610–617. Geostand. Newsl. 22, 7–13.

Kendall, B., Wang, J., Zheng, W., Romaniello, S.J., Over, D.J., Bennett, Y., Xing, L., Kunert, A., Boyes, C., Liu, J., 2020. Inverse correlation between the molybdenum and uranium isotope compositions of Upper Devonian black shales caused by changes in local depositional conditions rather than global ocean redox variations. Geochim. Cosmochim. Acta 287, 141–164.

Kigoshi, K., 1971. Alpha-recoil thorium-234: Dissolution into water and the uranium-234/uranium-238 disequilibrium in nature. Science 173, 47–48.

Kim, S.L., Eberle, J.J., Bell, D.M., Fox, D.A., Padilla, A., 2014. Evidence from shark teeth for a brackish Arctic Ocean in the Eocene greenhouse. Geology 42, 695–698.

Kim, S.L., Zeichner, S.S., Colman, A.S., Scher, H.D., Kriwet, J., Mörs, T., Huber, M., 2020. Probing the Ecology and Climate of the Eocene Southern Ocean with Sand Tiger Sharks *Striatolamia macrota*. Paleoceanogr. Paleoclimatology 35, 1–21.

Kipp, M.A., Li, H., Ellwood, M.J., John, S.G., Middag, R., Adkins, J.F., Tissot, F.L.H., 2022. ^{238}U, ^{235}U and ^{234}U in seawater and deep-sea corals: A high-precision reappraisal. Geochim. Cosmochim. Acta 336, 231–248.

Kipp, M.A., Tissot, F.L.H., 2022. Inverse methods for consistent quantification of seafloor anoxia using uranium isotope data from marine sediments. Earth Planet. Sci. Lett. 577, 117240.

Klug, S., Tütken, T., Wings, O., Pfretzschner, H.U., Martin, T., 2010. A Late Jurassic freshwater shark assemblage (Chondrichthyes, Hybodontiformes) from the southern Junggar Basin, Xinjiang, Northwest China. Palaeobiodiversity and Palaeoenvironments 90, 241–257.

Kocsis, L., Vennemann, T.W., Fontignie, D., 2007. Migration of sharks into freshwater systems during the Miocene and implications for Alpine paleoelevation. Geology 35, 451–454.

Kocsis, L., Vennemann, T.W., Hegner, E., Fontignie, D., Tütken, T., 2009. Constraints on Miocene oceanography and climate in the Western and Central Paratethys: O-, Sr-, and Nd-isotope compositions of marine fish and mammal remains. Palaeogeogr. Palaeoclimatol. Palaeoecol. 271, 117–129.

Kocsis, L., Ounis, A., Chaabani, F., Salah, N.M., 2013. Paleoenvironmental conditions and strontium isotope stratigraphy in the Paleogene Gafsa Basin (Tunisia) deduced from geochemical analyses of phosphatic fossils. Int. J. Earth Sci. 102, 1111–1129.

Kocsis, L., Gheerbrant, E., Mouflih, M., Cappetta, H., Yans, J., Amaghzaz, M., 2014. Comprehensive stable isotope investigation of marine biogenic apatite from the late Cretaceous-early Eocene phosphate series of Morocco. Palaeogeogr. Palaeoclimatol. Palaeoecol. 394, 74–88.

Kohn, M.J., Cerling, T.E., 2002. Stable Isotope Compositions of Biological Apatite. Rev. Mineral. Geochemistry 48, 455–488.

Kohn, M.J., Schoeninger, M.J., Barker, W.W., 1999. Altered states: Effects of diagenesis on fossil tooth chemistry. Geochim. Cosmochim. Acta 63, 2737–2747.

Kolodny, Y., Luz, B., Taylor, H.P., 1991. Oxygen isotopes in phosphates of fossil fish—Devonian to Recent, in: Stable Isotope Geochemistry: A Tribute to Samuel Epstein. The Geochemical Society, Special Publication, pp. 105–119.

Kolodny, Y., Luz, B., Navon, O., 1983. Oxygen isotope variations in phosphate of biogenic apatites, I. Fish bone apatite-rechecking the rules of the game. Earth Planet. Sci. Lett. 64, 398–404.

Kolodny, Y., Raab, M., 1988. Oxygen isotopes in phosphatic fish remains from Israel: Paleothermometry of tropical cretaceous and tertiary shelf waters. Palaeogeogr. Palaeoclimatol. 64, 59–67.

Ku, T.L., Mathieu, G.G., Knauss, K.G., 1977. Uranium in open ocean: concentration and isotopic composition. Deep Sea Research 24, 1005–1017.

Langmuir, D., 1978. Uranium solution-mineral equilibria at low temperatures with applications to sedimentary ore deposits. Geochim. Cosmochim. Acta 42, 547–569.

Lau, K.V., Maher, K., Altiner, D., Kelley, B.M., Kump, L.R., Lehrmann, D.J., Silva-Tamayo, J.C., Weaver, K.L., Yu, M., Payne, J.L., 2016. Marine anoxia and delayed Earth system recovery after the end-Permian extinction. Proc. Natl. Acad. Sci. u. s. a. 113, 2360–2365.

Lau, K.V., Hancock, L.G., Severmann, S., Kuzminov, A., Cole, D.B., Behl, R.J., Planavsky, N.J., Lyons, T.W., 2022. Variable local basin hydrography and productivity control the uranium isotope paleoredox proxy in anoxic black shales. Geochim. Cosmochim. Acta 317, 433–456.

Lécuyer, C., Grandjean, P., O'Neil, J.R., Cappetta, H., Martineau, F., 1993. Thermal excursions in the ocean at the Cretaceous-Tertiary boundary (northern Morocco): $\delta^{18}O$ record of phosphatic fish debris. Palaeogeogr. Palaeoclimatol. Palaeoecol. 105, 235–243.

Lécuyer, C., Picard, S., Garcia, J.P., Sheppard, S.M.F., Grandjean, P., Dromart, G., 2003. Thermal evolution of Tethyan surface waters during the Middle-Late Jurassic: Evidence from $\delta^{18}O$ values of marine fish teeth. Paleoceanography 18, 1076.

Lécuyer, C., Reynard, B., Grandjean, P., 2004. Rare earth element evolution of Phanerozoic seawater recorded in biogenic apatites. Chem. Geol. 204, 63–102.

Lécuyer, C., Amiot, R., Touzeau, A., Trotter, J., 2013. Calibration of the phosphate $\delta^{18}O$ thermometer with carbonate-water oxygen isotope fractionation equations. Chem. Geol. 347, 217–226.

LeGrande, A.N., Schmidt, G.A., 2006. Global gridded data set of the oxygen isotopic composition in seawater. Geophys. Res. Lett. 33, 1–5.

Li, D., Peng, J., Chew, D., Liang, Y., Hollings, P., Fu, Y., Dong, Y., Sun, X., 2023. Dating rare earth element enrichment in deep-sea sediments using U-Pb geochronology of bioapatite. Geology 51 (5), 428–433.

Li, H., Tissot, F.L.H., 2023. UID: The uranium isotope database. Chem. Geol. 618, 121221.

Livermore, B.D., Dahl, T.W., Bizzarro, M., Connelly, J.N., 2020. Uranium isotope compositions of biogenic carbonates – Implications for U uptake in shells and the application of the paleo-ocean oxygenation proxy. Geochim. Cosmochim. Acta 287, 50–64.

Longerich, H.P., Jackson, S.E., Günther, D., 1996. Laser ablation inductively coupled plasma mass spectrometric transient signal data acquisition and analyte concentration calculation. J. Anal. At. Spectrom. 11, 899–904.

Longinelli, A., 1966. Ratios of Oxygen-18: Oxygen-16 in phosphate and carbonate from living and fossil marine organisms. Nature 211, 923–927.

Martin, E.E., Haley, B.A., 2000. Fossil fish teeth as proxies for seawater Sr and Nd isotopes. Geochim. Cosmochim. Acta 64, 835–847.

Martin, E.E., Scher, H.D., 2004. Preservation of seawater Sr and Nd isotopes in fossil fish teeth: Bad news and good news. Earth Planet. Sci. Lett. 220, 25–39.

Martin, A.N., Markowska, M., Chivas, A.R., Weyer, S., 2023. Assessing the reliability of modern marine stromatolites as archives for the uranium isotope paleoredox proxy. Geochim. Cosmochim. Acta 345, 75–89.

McCormack, J., Griffiths, M.L., Kim, S.L., Shimada, K., Karnes, M., Maisch, H., Pederzani, S., Bourgon, N., Jaouen, K., Becker, M.A., Jöns, N., Sisma-Ventura, G., Straube, N., Pollerspöck, J., Hublin, J.J., Eagle, R.A., Tütken, T., 2022. Trophic position of *Otodus* megalodon and great white sharks through time revealed by zinc isotopes. Nat. Commun. 13, 1–10.

Miall, A.D., 1979. Mesozoic and Tertiary geology of Banks Island, Arctic Canada: the history of an unstable craton margin. Geological Survey of Canada, Ottawa, Canada.

Millard, A.R., Hedges, R.E.M., 1996. A diffusion-adsorption model of uranium uptake by archaeological bone. Geochim. Cosmochim. Acta 60, 2139–2152.

Miller, R.F., Cloutier, R., Turner, S., 2003. The oldest articulated chondrichthyan from the Early Devonian period. Nature 425, 501–504.

Mine, A.H., Waldeck, A., Olack, G., Hoerner, M.E., Alex, S., Colman, A.S., 2017. Microprecipitation and $\delta^{18}O$ analysis of phosphate for paleoclimate and biogeochemistry research. Chem. Geol. 460, 1–14.

Montoya-Pino, C., Weyer, S., Anbar, A.D., Pross, J., Oschmann, W., van de Schootbrugge, B., Arz, H.W., 2010. Global enhancement of ocean anoxia during oceanic anoxic event 2: A quantitative approach using U isotopes. Geology 38, 315–318.

Moreno, E.C., Kresak, M., Zahradnik, R.T., 1974. Fluoridated hydroxyapatite solubility and caries formation. Nature 247, 64–65.

Noordmann, J., Weyer, S., Montoya-Pino, C., Dellwig, O., Neubert, N., Eckert, S., Paetzel, M., Böttcher, M.E., 2015. Uranium and molybdenum isotope systematics in modern euxinic basins: Case studies from the central Baltic Sea and the Kyllaren fjord (Norway). Chem. Geol. 396, 182–195.

Noordmann, J., Weyer, S., Georg, R.B., Jöns, S., Sharma, M., 2016. $^{238}U/^{235}U$ isotope ratios of crustal material, rivers and products of hydrothermal alteration: new insights on the oceanic U isotope mass balance. Isotopes Environ. Health Stud. 52, 141–163.

Ochoa, D., Salas-Gismondi, R., DeVries, T.J., Baby, P., de Muizon, C., Altamirano, A., Barbosa-Espitia, A., Foster, D.A., Quispe, K., Cardich, J., 2021. Late Neogene evolution of the Peruvian margin and its ecosystems: a synthesis from the Sacaco record. Int. J. Earth Sci. 110, 995–1025.

Ounis, A., Kocsis, L., Chaabani, F., Pfeifer, H.R., 2008. Rare earth elements and stable isotope geochemistry ($\delta^{13}C$ and $\delta^{18}O$) of phosphorite deposits in the Gafsa Basin. Tunisia. Palaeogeogr. Palaeoclimatol. Palaeoecol. 268, 1–18.

Owens, S.A., Buesseler, K.O., Sims, K.W.W., 2011. Re-evaluating the 238U-salinity relationship in seawater: Implications for the $^{238}U-^{234}Th$ disequilibrium method. Mar. Chem. 127, 31–39.

Padilla, A., Eberle, J.J., Gottfried, M.D., Sweet, A.R., Hutchison, J.H., 2014. A sand tiger shark-dominated fauna from the Eocene Arctic greenhouse. J. Vertebr. Paleontol. 34, 1307–1316.

Phan, T.T., Gardiner, J.B., Capo, R.C., Stewart, B.W., 2018. Geochemical and multi-isotopic ($^{87}Sr/^{86}Sr$, $^{143}Nd/^{144}Nd$, $^{238}U/^{235}U$) perspectives of sediment sources, depositional conditions, and diagenesis of the Marcellus Shale, Appalachian Basin, USA. Geochim. Cosmochim. Acta 222, 187–211.

Picard, S., Garcia, J.P., Lécuyer, C., Sheppard, S.M.F., Cappetta, H., Emig, C.C., 1998. $\delta^{18}O$ values of coexisting brachiopods and fish: Temperature differences and estimates of paleo-water depths. Geology 26, 975–978.

Pike, A.W.G., Hedges, R.E.M., 2001. Sample geometry and U uptake in archaeological teeth: Implications for U-series and ESR dating. Quat. Sci. Rev. 20, 1021–1025.

Polyak, V.J., Curry, B.H., Lavery, D.J., Strasberg, Z.L., Cutler, S., Song, W., Crossey, L.J., Karlstrom, K.E., Asmerom, Y., 2023. Large negative $\delta^{238}U$ anomalies in endogenic-type travertine systems. Geology 51, 1048–1052.

Pucéat, E., Lécuyer, C., Sheppard, S.M.F., Dromart, G., Reboulet, S., Grandjean, P., 2003. Thermal evolution of Cretaceous Tethyan marine waters inferred from oxygen isotope composition of fish tooth enamels. Paleoceanography 18, 1–12.

Reynard, B., Lécuyer, C., Grandjean, P., 1999. Crystal-chemical controls on rare-earth element concentrations in fossil biogenic apatites and implications for paleoenvironmental reconstructions. Chem. Geol. 155, 233–241.

Richter, S., Eykens, R., Kühn, H., Aregbe, Y., Verbruggen, A., Weyer, S., 2010. New average values for the n(^{238}U)/n(^{235}U) isotope ratios of natural uranium standards. Int. J. Mass Spectrom. 295, 94–97.

Robinson, L.F., Belshaw, N.S., Henderson, G.M., 2004. U and Th concentrations and isotope ratios in modern carbonates and waters from the Bahamas. Geochim. Cosmochim. Acta 68, 1777–1789.

Rolison, J.M., Stirling, C.H., Middag, R., Rijkenberg, M.J.A., 2017. Uranium stable isotope fractionation in the Black Sea: Modern calibration of the $^{238}U/^{235}U$ paleo-redox proxy. Geochim. Cosmochim. Acta 203, 69–88.

Romaniello, S.J., Herrmann, A.D., Anbar, A.D., 2013. Uranium concentrations and $^{238}U/^{235}U$ isotope ratios in modern carbonates from the Bahamas: Assessing a novel paleoredox proxy. Chem. Geol. 362, 305–316.

Rudnick, R.L., Gao, S., 2014. Composition of the Continental Crust. Treatise on Geochemistry. Elsevier 1–51.

Schmitz, B., Aberg, G., Werdelin, L., Forey, P., Bendix-Almgreen, S.E., 1991. $^{87}Sr/^{86}Sr$, Na, F, Sr, and La in skeletal fish debris as a measure of the paleosalinity of fossil-fish habitats. Geol. Soc. Am. Bull. 103, 786–794.

Schmitz, B., Ingram, S.L., Dockery, D.T., Åberg, G., 1997. Testing $^{87}Sr/^{86}Sr$ as a paleosalinity indicator on mixed marine, brackish-water and terrestrial vertebrate skeletal apatite in late Paleocene-early Eocene near-coastal sediments. Mississippi. Chem. Geol. 140, 275–287.

Sharp, Z.D., Atudorei, V., Furrer, H., 2000. The effect of diagenesis on oxygen isotope ratios of biogenic phosphates. Am. J. Sci. 300, 222–237.

Shaw, H.F., Wasserburg, G.J., 1985. Sm-Nd in marine carbonates and phosphates: Implications for Nd isotopes in seawater and crustal ages. Geochim. Cosmochim. Acta 49, 503–518.

Shemesh, A., Kolodny, Y., Luz, B., 1983. Oxygen isotope variations in phosphate of biogenic apatites, II. Phosphorite Rocks. Earth Planet. Sci. Lett. 64, 405–416.

Staudigel, H., Doyle, P., Zindler, A., 1985. Sr and Nd isotope systematics in fish teeth. Earth Planet. Sci. Lett. 76, 45–56.

Stirling, C.H., Andersen, M.B., Potter, E.-K., Halliday, A.N., 2007. Low-temperature isotopic fractionation of uranium. Earth Planet. Sci. Lett. 264, 208–225.

Sweet, A. R. 2012. Applied research report on 5 outcrop samples collected by Andrew Miall from northern Banks Island. NWT (NTS Map Sheets 098E/01, 08, 09): Geological Survey of Canada Paleontological report ARS-2012-01.

Tarhan, L.G., Planavsky, N.J., Wang, X., Bellefroid, E.J., Droser, M.L., Gehling, J.G., 2018. The late-stage "ferruginization" of the Ediacara Member (Rawnsley Quartzite, South Australia): Insights from uranium isotopes. Geobiology 16, 35–48.

Thomas, D.B., McGoverin, C.M., Fordyce, R.E., Frew, R.D., Gordon, K.C., 2011. Raman spectroscopy of fossil bioapatite - A proxy for diagenetic alteration of the oxygen isotope composition. Palaeogeogr. Palaeoclimatol. Palaeoecol. 310, 62–70.

Tissot, F.L.H., Dauphas, N., 2015. Uranium isotopic compositions of the crust and ocean: Age corrections, U budget and global extent of modern anoxia. Geochim. Cosmochim. Acta 167, 113–143.

Tissot, F.L.H., Dauphas, N., Grossman, L., 2016. Origin of uranium isotope variations in early solar nebula condensates. Sci. Adv. 2, e1501400.

Tissot, F.L.H., Dauphas, N., Grove, T.L., 2017. Distinct $^{238}U/^{235}U$ ratios and REE patterns in plutonic and volcanic angrites: Geochronologic implications and evidence for U isotope fractionation during magmatic processes. Geochim. Cosmochim. Acta 213, 593–617.

Tissot, F.L.H., Chen, C., Go, B.M., Naziemiec, M., Healy, G., Bekker, A., Swart, P.K., Dauphas, N., 2018. Controls of eustasy and diagenesis on the $^{238}U/^{235}U$ of carbonates and evolution of the seawater ($^{234}U/^{238}U$) during the last 1.4 Myr. Geochim. Cosmochim. Acta 242, 233–265.

Tissot, F.L.H., Ibanez-Mejia, M., Boehnke, P., Dauphas, N., McGee, D., Grove, T.L., Harrison, T.M., 2019. $^{238}U/^{235}U$ measurement in single-zircon crystals: Implications for the Hadean environment, magmatic differentiation and geochronology. J. Anal. at. Spectrom. 34, 2035–2052.

Toyoda, K., Tokonami, M., 1990. Diffusion of rare-earth elements in fish teeth from deep-sea sediments. Nature 345, 607–609.

Trotter, J.A., Eggins, S.M., 2006. Chemical systematics of conodont apatite determined by laser ablation ICPMS. Chem. Geol. 233, 196–216.

Trueman, C.N., Tuross, N., 2002. Trace Elements in Recent and Fossil Bone Apatite. Rev. Mineral. Geochemistry 48, 489–521.

Tütken, T., Vennemann, T.W., Pfretzschner, H.U., 2011. Nd and Sr isotope compositions in modern and fossil bones - Proxies for vertebrate provenance and taphonomy. Geochim. Cosmochim. Acta 75, 5951–5970.

Tütken, T., Weber, M., Zohar, I., Helmy, H., Bourgon, N., Lernau, O., Jochum, K.P., Sisma-Ventura, G., 2020. Strontium and Oxygen Isotope Analyses Reveal Late Cretaceous Shark Teeth in Iron Age Strata in the Southern Levant. Front. Ecol. Evol. 8, 1–25.

Vennemann, T.W., Hegner, E., 1998. Oxygen, strontium, and neodymium isotope composition of fossil shark teeth as a proxy for the palaeoceanography and palaeoclimatology of the Miocene northern Alpine Paratethys. Palaeogeogr. Palaeoclimatol. Palaeoecol. 142, 107–121.

Vennemann, T.W., Hegner, E., Cliff, G., Benz, G.W., 2001. Isotopic composition of recent shark teeth as a proxy for environmental conditions. Geochim. Cosmochim. Acta 65, 1583–1599.

Waddell, L.M., Moore, T.C., 2008. Salinity of the Eocene Arctic Ocean from oxygen isotope analysis of fish bone carbonate. Paleoceanography 23, 1–14.

Wang, X., Planavsky, N.J., Reinhard, C.T., Hein, J.R., Johnson, T.M., 2016. A Cenozoic seawater redox record derived from ^{238}U/^{235}U in ferromanganese crusts. Am. J. Sci. 315, 64–83.

Weyer, S., Anbar, A.D., Gerdes, A., Gordon, G.W., Algeo, T.J., Boyle, E.A., 2008. Natural fractionation of ^{238}U/^{235}U. Geochim. Cosmochim. Acta 72, 345–359.

White, D.A., Elrick, M., Romaniello, S., Zhang, F., 2018. Global seawater redox trends during the Late Devonian mass extinction detected using U isotopes of marine limestones. Earth Planet. Sci. Lett. 503, 68–77.

Zazzo, A., Lécuyer, C., Mariotti, A., 2004a. Experimentally controlled carbon and oxygen isotope exchange between bioapatites and water under inorganic and microbially-mediated conditions. Geochim. Cosmochim. Acta 68, 1–12.

Zazzo, A., Lécuyer, C., Sheppard, S.M.F., Grandjean, P., Mariotti, A., 2004b. Diagenesis and the reconstruction of paleoenvironments: A method to restore original δ^{18}O values of carbonate and phosphate from fossil tooth enamel. Geochim. Cosmochim. Acta 68, 2245–2258.

Zhang, Q., Ding, L., Chen, X., Brennecka, G.A., Sun, Y., Ma, X., Gao, B., Zhang, Q., Willems, H., 2023. The large decline in carbonate δ^{238}U from a PETM section at Tingri (South Tibet) was driven by local sea-level changes, not global oceanic anoxia. Earth Planet. Sci. Lett. 612, 118164.

Zhang, F., Xiao, S., Romaniello, S.J., Hardisty, D., Li, C., Melezhik, V., Pokrovsky, B., Cheng, M., Shi, W., Lenton, T.M., Anbar, A.D., 2019. Global marine redox changes drove the rise and fall of the Ediacara biota. Geobiology 17, 594–610.

Zhang, F., Lenton, T.M., del Rey, Á., Romaniello, S.J., Chen, X., Planavsky, N.J., Clarkson, M.O., Dahl, T.W., Lau, K.V., Wang, W., Li, Z., Zhao, M., Isson, T., Algeo, T.J., Anbar, A.D., 2020. Uranium isotopes in marine carbonates as a global ocean paleoredox proxy: A critical review. Geochim. Cosmochim. Acta 287, 27–49.